Positronium Decay into a Photon and Neutrinos

by

Andrzej Pokraka

A thesis submitted in partial fulfillment of the requirements for the degree of

Master of Science

Department of Physics

University of Alberta

Abstract

We determine the rates, photon energy and angular distributions of positronium decays into a photon and a neutrino-antineutrino pair, Ps $\to \gamma\nu_\ell\bar{\nu}_\ell$. We find that both positronium spin states have access to this decay channel, contrary to a previously published result. The low-energy tails of the spectra are shown to be sensitive to binding effects in positronium and agree with Low's theorem. Additionally, we find a connection between the behaviour of the soft photon spectrum in both o-Ps $\to \gamma\nu_\ell\bar{\nu}_\ell$ and o-Ps $\to 3\gamma$ decays, and the Stark effect.

Preface

This thesis is the original work of Andrzej Pokraka with guidance from Professor Czarnecki. Material from this thesis has been published as: Andrzej Pokraka and Andrzej Czarnecki, "Positronium decay into a photon and neutrinos", Phys. Rev. **D94**, 113012 (2016).

Acknowledgements

I thank Professor Czarnecki for his expert guidance, mentorship, support and patience throughout my master's program. Sasha Serediak, Ed and Michele Pokraka, I am appreciative of your understanding, patience and support.

I also thank the Max Planck Institut für Physik, where part of this work was completed, for their hospitality.

I am very grateful to have held a NSERC CGS-M scholarship during the completion of this work.

Contents

List of Tables

List of Figures

List of Abbreviations

List of commonly used abbreviations

Positronium	Ps
Parapositronium	p-Ps
Orthopositronium	o-Ps
Quantum electrodynamics	QED
Non-relativistic effective field theory	NREFT
Charge conjugation	C
Parity	P
Time reversal	T

Chapter 1

Introduction

Positronium (Ps), the bound state of an electron and its antiparticle, is a metastable leptonic atom. It is the lightest known atom and in many ways resembles hydrogen. Like hydrogen, Ps can form two spin states: the singlet parapositronium (p-Ps) and the triplet orthopositronium (o-Ps).

Decays of Ps can be precisely described within pure quantum electrodynamics (QED); the only limitation being the computational complexity of the higher orders in the expansion in the fine structure constant $\alpha \simeq 1/137$. Despite this complexity, many corrections in higher orders have been calculated [1, 2, 3, 4, 5, 6, 7, 8, 9, 10, 11, 12, 13].

While the dominant decay modes of Ps are purely photonic, weak interactions can transform Ps into final states involving neutrinos [14, 15, 16, 17, 18, 19]. Recently, Ref. [20] examined the exotic decay of Ps into a photon and a neutrino-antineutrino pair $\text{Ps} \to \gamma\nu_\ell\bar{\nu}_\ell$, and claimed that only p-Ps can decay in this way. On the other hand, Ref. [14] stated that o-Ps can decay into such a final state, even estimating its branching ratio.

This thesis addresses the apparent contradiction between Refs. [20] and [14]. We calculate the $\text{Ps} \to \gamma\nu_\ell\bar{\nu}_\ell$ decay rates and photon spectra for both p-Ps and o-Ps (chapter 2). We find that both p-Ps and o-Ps have access to the $\text{Ps} \to \gamma\nu_\ell\bar{\nu}_\ell$ decay mode. In

addition to establishing that the o-Ps decay rate is non-zero, we find differences between our calculated p-Ps rate and spectrum and those of Ref. [20]. We calculate the angular distributions of Ps $\to \gamma\nu_\ell\bar{\nu}_\ell$ decays in chapter 3.

It is easy to mislead oneself into thinking that only one Ps spin state can decay into $\gamma\bar{\nu}\nu$, since none of the previously studied final states was accessible to both. Due to the conservation of charge-conjugation (C) in pure QED, o-Ps decays into an odd number of photons and p-Ps into an even number. However in the theory of weak interactions, the weak bosons couple to both the C-odd vector and the C-even axial current. Thus, p-Ps can decay into a photon and a neutrino pair by a vector coupling (analogous to its main $\gamma\gamma$ decay) while o-Ps can decay into the same final state through an axial coupling.

In three-body channels, the energy of the decay products has an extended distribution. The low-energy tail is sensitive to binding effects; such effects have been determined in the three-photon decay of o-Ps [21, 22, 23, 24]. We find an analogous phenomenon in Ps $\to \gamma\nu_\ell\bar{\nu}_\ell$ decays. Unlike the 3γ decay accessible only to o-Ps, in Ps $\to \gamma\nu_\ell\bar{\nu}_\ell$ decays, one can compare the low-energy behaviour of both the p-Ps and o-Ps decays. In chapter 5, we employ the non-relativistic effective field theory (NREFT) methods of [22, 23, 24] to explain how binding effects connect the linear behaviour of the spectra found in chapter 2 with the cubic behaviour at extremely low energy, predicted by Low's theorem [25] (chapter 4).

Before proceeding to the detailed calculations starting in chapter 2, we summarize some basic properties of positronium. This includes Ps wave functions and energy levels (section 1.1), discrete symmetries (section 1.2), QED decay modes of Ps (section 1.3) and weak decays of Ps (section 1.4).

1.1 Wave functions and energy levels of Ps

The total wave function of Ps is the probability amplitude that Ps will be in a given configuration. To first approximation, the total wavefunction is the product of the spatial wave function, ψ_{nlm_l}, and the spinor (spin wave function), η_{sm_s},

$$\Psi_{nlm_l;sm_s}(\mathbf{x}) = \psi_{nlm_l}(\mathbf{x})\eta_{sm_s}, \tag{1.1}$$

where n, l, m_l, s and m_s are the quantum numbers that characterize a particular configuration or state. The energy levels are the energies associated with a given state of Ps.

Since Ps is a non-relativistic system, its spatial wave functions and energy levels are given by the energy eigenfunctions and energy eigenvalues of the Schrödinger equation for Ps. To first approximation, Ps is described by the Schrödinger equation for a particle of electric charge e and reduced mass $\mu = m/2$ in the Coulomb potential $V(|\mathbf{x}|) = -\alpha/|\mathbf{x}|$ where e (< 0) is the electron charge, m is the electron mass, $\alpha \approx 1/137$ is the fine structure constant and $\mathbf{x}$ is the separation distance between the electron and positron in Ps (note, we work in natural units where $\hbar = c = 1$). Instead of directly solving the Ps Schrödinger equation, the energy eigenfunctions and energy eigenvalues of Ps can be obtained by taking advantage of the similarity between the Schrödinger equation for Ps and that for hydrogen.

Specifically, the Ps spatial wave functions can be obtained by replacing the hydrogen Bohr radius with the Ps Bohr radius in the hydrogen energy eigenfunctions[1]. These wave functions are characterized by the principal quantum number (or energy quantum number), n, the orbital angular momentum quantum number, l, and the orbital angular

[1]A detailed analysis of the wave functions and energy levels for hydrogen can be found in any elementary text on quantum mechanics (e.g., Ref. [26]) and are therefore not duplicated here.

momentum projection quantum number, m_l. The spatial wave functions are

$$\psi_{nlm_l}(\mathbf{x}) = \sqrt{\left(\frac{2}{na}\right)^3 \frac{(n-l-1)!}{2n\left[(n+1)!\right]^3}} e^{-|\mathbf{x}|/na} \times \left(\frac{2|\mathbf{x}|}{na}\right)^l L^{2l+1}_{n-l-1}\left(\frac{2|\mathbf{x}|}{na}\right) Y_l^m(\theta,\phi), \tag{1.2}$$

where $a = 2/m\alpha$ is the Bohr radius of Ps, L^m_{n-m} are associated Laguerre polynomials and $Y_l^{m_l}$ are spherical harmonics. The ground state wave function, $\psi_0(\mathbf{x}) \equiv \psi_{100}(\mathbf{x})$, is the wave function of the $n = 1$, $l = m_l = 0$ state and is frequently used in our analysis of the Ps $\to \gamma\nu_\ell\bar{\nu}_\ell$ decay.

In addition to the spatial wavefunction, Ps has two spin states: the singlet state, p-Ps, and the triplet state, o-Ps. The Ps spinor contains the spin information of Ps and is the tensor product of the electron spinor, ϕ, and positron spinor, χ,

$$\eta_{sm_s} \equiv \phi\chi^\dagger = \begin{cases} \mathbb{I}_{2\times 2}/\sqrt{2} & \text{for } s = 0 \text{ (p-Ps)} \\ \boldsymbol{\xi}_{m_s}\cdot\boldsymbol{\sigma}/\sqrt{2} & \text{for } s = 1 \text{ (o-Ps).} \end{cases} \tag{1.3}$$

where s is the spin quantum number and m_s is the spin projection quantum number. Here, $\mathbb{I}_{2\times 2}$ is the 2 by 2 identity matrix, $\boldsymbol{\sigma}$ are the Pauli matrices and $\boldsymbol{\xi}_{m_s}$ are the o-Ps spin vectors,

$$\boldsymbol{\xi}_{m_s} = \begin{cases} (-1,-i,0)/\sqrt{2} & \text{for } m_s = 1 \\ (0,0,1) & \text{for } m_s = 0 \\ (1,-i,0)/\sqrt{2} & \text{for } m_s = -1. \end{cases} \tag{1.4}$$

Now that we have determined the spatial wave function and the spinors, these can be used to obtain the total Ps wave function using equation (1.1).

The energy levels of Ps can be obtained by replacing the electron mass with the

reduced mass of Ps in the hydrogen energy eigenvalues,

$$E_n(\text{Ps}) = -\frac{m\alpha^2}{4n^2}. \tag{1.5}$$

The binding energy of Ps is the energy needed to break Ps into a free electron and free positron. It is the negative of the ground state energy, $-E_1 = m\alpha^2/4$. In order to understand binding effects in the photon spectrum, we calculate the photon spectra of Ps $\to \gamma\nu_\ell\bar{\nu}_\ell$ decays for photons with energies less than the Ps binding energy (chapter 5).

Relativistic corrections to the kinetic energy as well as interactions involving the electron and positron spins induce small corrections to the energy levels and spatial wavefunctions of Ps.

The spin-orbit interaction yields corrections of order $\mathcal{O}(\alpha^2)$. These corrections originate from the interaction of the electron's/positron's magnetic dipole moment with the magnetic field created by the orbiting electron/positron. The spin-orbit corrections break the energy degeneracy in l (i.e., the energies become l dependent) resulting in what is known as the fine structure of Ps.

The spin-spin interaction contributes corrections of order $\mathcal{O}(\alpha^4)$. These corrections originate from the interaction of the dipole moments of the electron and positron. The spin-spin corrections distinguish the energies of p-Ps from the energies of o-Ps. This energy splitting is known as the hyper-fine structure of Ps.

1.2 Discrete symmetries

Discrete symmetries place restrictions on the allowed decays of Ps. For example, discrete symmetries determine whether decays, such as o-Ps $\to \gamma\nu_\ell\bar{\nu}_\ell$, can occur.

There are three discrete symmetries in the standard model of particle physics: charge conjugation (C) – the exchange of particles with antiparticles; parity (P) – the inversion of spatial coordinates; time reversal (T) – inversion of the time coordinate. If an interaction

Table 1.1: P and C eigenvalues of the total Ps wave function, $\Psi_{nlm_l;sm_s}$. Here, l is the orbital angular momentum quantum number and s is the spin angular momentum quantum number.

Discrete Transform	Ps Eigenvalue
P	$(-1)^{l+1}$
C	$(-1)^{l+s}$

is invariant under a discrete symmetry (or a composition of discrete symmetries) and if the initial state is an eigenstate of the discrete symmetry, then the final state, after interaction, must be an eigenstate of the symmetry operator with the same eigenvalue.

In order to understand the restrictions discrete symmetries place on Ps decays, we need to determine the C, P and T eigenvalues of Ps.

The P eigenvalue of Ps is the product of the respective P eigenvalues of the spatial wave function and spinor[2]. To obtain the P eigenvalue of the spatial wave function, we begin by inverting the spatial coordinates in equation (1.2). The only part of the spatial wave function that is sensitive to such an inversion is the spherical harmonic, $Y_{lm}(\theta,\phi) \rightarrow (-1)^l Y_{lm}(\theta,\phi)$. Thus, the P eigenvalues of the spatial wave functions are $(-1)^l$. The P eigenvalue of the Ps spinor is a product of the intrinsic parity of the electron and positron. Since the electron has an intrinsic parity of 1 and the positron has an intrinsic parity of (-1), the Ps spinor transforms as $\eta_{sm_s} \rightarrow -\eta_{sm_s}$ under P [27, 28, 29]. Therefore, the P eigenvalue of the total Ps wave function is $(-1)^{l+1}$, or equivalently under P, the total wave function transforms as

$$\Psi_{nlm_l;sm_s}(\mathbf{x}) \xrightarrow{P} (-1)^{l+1}\Psi_{nlm_l;sm_s}(\mathbf{x}). \tag{1.6}$$

To determine the C eigenvalue of Ps, we note that application of C is equivalent to the application of P and interchanging the positron and electron in the Ps spinor [30].

[2]The C and T eigenvalues can also be obtained in the same manner. However, we chose a simpler alternative approach.

The p-Ps (o-Ps) spinor is antisymmetric (symmetric) under the exchange of electron and positron, contributing a factor of $(-1)^{s+1}$ to the C eigenvalue. Multiplying this with the P eigenvalue yields the C eigenvalue, $(-1)^{s+l}$. Therefore, the total Ps wave function transforms as

$$\Psi_{nlm_l;sm_s}(\mathbf{x}) \xrightarrow{C} (-1)^{s+l}\Psi_{nlm_l;sm_s}(\mathbf{x}). \tag{1.7}$$

The time-reversal operator is an anti-unitary operator that reverses the direction of the 3-momentum and spin of a particle [29]. Acting on the total Ps wavefunction, T sends the position space wavefunction to its complex conjugate $\psi_{nlm_l} \to \psi^*_{nlm_l} = (-1)^{m_l}\psi_{n,l,-m_l}$ and flips the spin of the electron and positron in the Ps spinor $\eta_{sm_s} \to (-1)^{s+1}\eta_{s,-m_s}$. Combining the above, we obtain the transformation rule for the total Ps wavefunction under T

$$\Psi_{nlm_l;sm_s}(\mathbf{x}) \xrightarrow{T} (-1)^{m_l+s+1}\Psi_{n,l,-m_l;s,-m_s}(\mathbf{x}). \tag{1.8}$$

Notice that the Ps state is not an eigenstate of the time-reversal operator.

Since the Ps state is not an eigenstate of T, only the discrete symmetries of P and C restrict the decay modes of Ps. The P and C eigenvalues of the total Ps wave function are listed in Table 1.1.

1.3 QED decay modes of Ps

Within QED, Ps can only decay into photons. Furthermore, the decays of p-Ps and o-Ps are restricted to different final states by C conservation. In other words, the allowed decay modes must have the same C eigenvalue for the initial and final state.

To determine the allowed decay modes, we equate the C eigenvalue for Ps and the C eigenvalue for a state of N photons, and determine the valid values of N. Since the C

eigenvalue of a photon is -1[3] a final state with N photons has a C eigenvalue of $(-1)^N$ [30]. Equating the C eigenvalue of the initial state (Table 1.1) and that of the final state (N photons) yields the condition

$$(-1)^{l+s} = (-1)^N \implies l + s \equiv N \pmod 2. \tag{1.9}$$

That is, for an orbital angular momentum, l, p-Ps must decay into $l + 2n$ photons while o-Ps must decay into $l + 2n + 1$ photons where n is a nonnegative integer. These are called the selection rules for QED decay modes of Ps. Note, the single photon decay is forbidden by momentum conservation.

The dominant ($n = 1$) decay modes of Ps are: p-Ps $\to 2\gamma$ and o-Ps $\to 3\gamma$. These decay modes determine the lifetime of Ps. To first order, the Ps lifetimes are given by the corresponding electron-positron annihilation rate at rest, $e^+e^- \to 2\gamma$, for p-Ps [31] and $e^+e^- \to 3\gamma$ for o-Ps [32] (see Fig. 1.3). Explicitly, the lifetimes of Ps are

$$\tau(\text{Ps}) = \begin{cases} \frac{2}{m_e\alpha^5} \approx 10^{-10}\text{s} & \text{for p-Ps} \\ \\ \frac{9\pi}{2(\pi^2-9)m_e\alpha^6} \approx 10^{-7}\text{s} & \text{for o-Ps} \end{cases} \tag{1.10}$$

which are the inverses of the decay rates

$$\Gamma(\text{Ps}) = \begin{cases} \frac{m_e\alpha^5}{2} \approx 10^{10}\text{s}^{-1} & \text{for p-Ps} \\ \\ \frac{2(\pi^2-9)m_e\alpha^6}{9\pi} \approx 10^{7}\text{s}^{-1} & \text{for o-Ps.} \end{cases} \tag{1.11}$$

The branching ratio of the decay Ps $\to X$, for some final state X, is a measure of how often that decay occurs relative to all possible decays. It is defined as the ratio of the Ps $\to X$ decay rate and the total decay rate of Ps. Since the total decay rate is

[3]Intuitively, we can see this by considering the classical electromagnetic field, A_μ; when the sign of the charge and charge density is reversed, $A_\mu \to -A_\mu$.

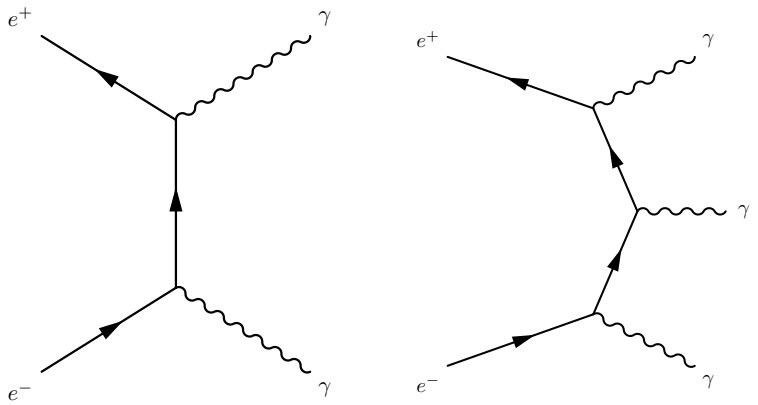

Figure 1.1: Feynman graphs for (a) $e^+e^- \to 2\gamma$ and (b) $e^+e^- \to 3\gamma$ annihilation.

approximately the same as the decay rate of the dominant mode, the branching ratios for p-Ps $\to X$ and o-Ps $\to X$ are approximately

$$\begin{aligned} \mathrm{Br}(\text{p-Ps} \to X) &\approx \frac{\Gamma(\text{p-Ps} \to X)}{\Gamma(\text{p-Ps} \to 2\gamma)}, \\ \mathrm{Br}(\text{o-Ps} \to X) &\approx \frac{\Gamma(\text{o-Ps} \to X)}{\Gamma(\text{o-Ps} \to 3\gamma)}. \end{aligned} \tag{1.12}$$

The Ps $\to \gamma\nu_\ell\bar{\nu}_\ell$ branching ratios are calculated in chapter 2.

1.4 Weak decays of Ps

Weak interactions introduce new decay modes for Ps with final states that include both photons and neutrinos. The theory of weak interactions, unlike QED, breaks both C- and P-symmetry but approximately conserves the composite symmetry CP[4]. The breaking of C-symmetry opens the possibility of C-violating photonic decay modes such as p-Ps $\to 3\gamma$ and o-Ps $\to 4\gamma$ as well as C-violating photon-neutrino decays such as o-Ps $\to \gamma\nu_\ell\bar{\nu}_\ell$. These and other novel decays make Ps an interesting tool for studying C-violating effects.

While interesting, weak decays of Ps are heavily suppressed because the electron

[4]While processes involving all three generations of leptons can break CP, they are not important for the decays we consider. Therefore, we take CP to be an exact symmetry of the weak interaction.

mass is tiny compared to the mass of the force mediating Z- and W-bosons. Since the amplitudes for weak decays are proportional to $\mathrm{G_F}m^2 \approx 3 \cdot 10^{-12}$ [14] (where $\mathrm{G_F} \simeq 1.166 \cdot 10^{-5}/\mathrm{GeV}^2$ is the Fermi constant [33]), these decays have exceptionally small decay rates and branching ratios. For example, Ref. [17] considers the decay of Ps into a neutrino-antineutrino pair ($\mathrm{Ps} \to \nu_\ell \bar{\nu}_\ell$). It reports that only o-Ps can undergo such a decay. This decay has rates

$$\Gamma(\text{o-Ps} \to \nu_\ell \bar{\nu}_\ell) = \begin{cases} \frac{G_\mathrm{F}^2 \alpha^3 m_\mathrm{e}^5}{24\pi}(1 + 4\sin^2\theta_W) \approx 7.2 \cdot 10^{-11}\mathrm{s}^{-1} & \text{for } \ell = e \\ \frac{G_\mathrm{F}^2 \alpha^3 m_\mathrm{e}^5}{24\pi}(1 - 4\sin^2\theta_W) \approx 1.8 \cdot 10^{-12}\mathrm{s}^{-1} & \text{for } \ell = \nu, \tau, \end{cases} \tag{1.13}$$

and branching ratios

$$\mathrm{Br}(\text{o-Ps} \to \nu_\ell \bar{\nu}_\ell) = \begin{cases} 9.5 \cdot 10^{-21} & \text{for } \ell = e \\ 6.2 \cdot 10^{-18} & \text{for } \ell = \nu, \tau. \end{cases} \tag{1.14}$$

Even though these decays cannot be detected today [19], such rare standard model decays will be important in the search for new beyond the standard model physics as experimental sensitivity increases.

As in the $\mathrm{Ps} \to \nu_\ell \bar{\nu}_\ell$ decay outlined above, previous research has found that weak (as well as QED) decays were exclusively accessible to either p-Ps or o-Ps. It is, therefore, easy to assume that only one Ps spin state can decay into $\gamma \nu_\ell \bar{\nu}_\ell$, the subject of our research. However, it is not obvious that this assumption should be true since weak interactions break C-symmetry.

We hypothesise that p-Ps can decay into a photon and a neutrino pair through a C-even vector coupling (analogous to its main 2γ decay) while o-Ps can decay into the same final state through a C-odd axial coupling. This hypothesis will be tested in chapter 2 where we compute the p-Ps $\to \gamma \nu_\ell \bar{\nu}_\ell$ and o-Ps $\to \gamma \nu_\ell \bar{\nu}_\ell$ decay rates.

Chapter 2

Ps $\to \gamma\nu_\ell\bar{\nu}_\ell$ decay rates and photon spectra

The relevant $e^+e^- \to \gamma\nu_\ell\bar{\nu}_\ell$ annihilation graphs for Ps $\to \gamma\nu_\ell\bar{\nu}_\ell$ decays are presented in Fig. 2. The photon is emitted off the initial electron or positron before the e^+e^- pair annihilates into a neutrino-antineutrino pair via Z or W boson exchange. The s-channel Z-boson exchange (Fig. 2.1(a)) contributes to the amplitude for all lepton flavors, ℓ, while the t-channel W-boson exchange (Fig. 2.1(b)) contributes to the amplitude only when $\ell = e$. The photon can also be emitted off of an internal charged W boson (Fig. 2.1(c)); since this process is suppressed by an additional factor of $m^2/M_{\rm W}^2 \approx 4 \cdot 10^{-11} \ll 1$ where m is the electron mass and $M_{\rm W}$ is the W-boson mass, it is ignored in our calculations.

We begin by calculating both Ps $\to \gamma\nu_\ell\bar{\nu}_\ell$ decay amplitudes. The initial incoming 4-momenta of the electron and positron are denoted by p_1 and p_2 while outgoing 4-momenta are denoted by k_i where k_1 is the 4-momentum of the neutrino, k_2 the anti-neutrino and k_γ the photon. Since the Ps binding energy is small, $\mathcal{O}(m\alpha^2)$, compared to the rest mass of the initial leptons, their average kinetic energy is negligible. Therefore, we take the initial electron and positron to be at rest with 4-momentum $p_1 = p_2 = p = (m, \mathbf{0})$. Similarly, the momenta of the virtual Z and W bosons are also negligible compared to

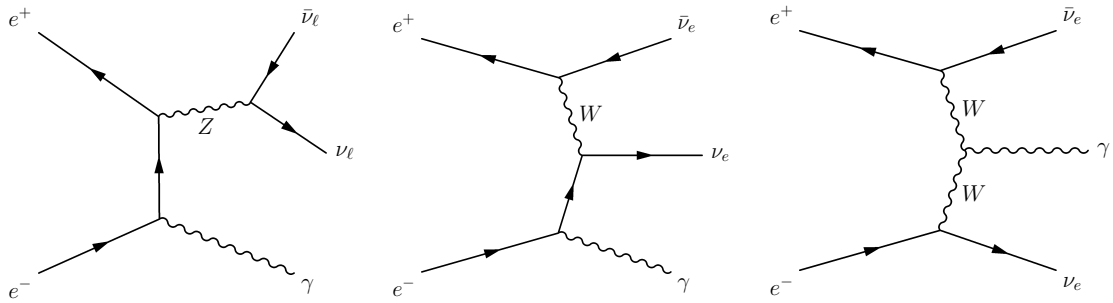

Figure 2.1: Feynman graphs that contribute to the $e^+e^- \to \gamma\nu_\ell\bar{\nu}_\ell$ annihilation amplitudes relevant for Ps $\to \gamma\nu_\ell\bar{\nu}_\ell$ decays ($\ell = e, \mu, \tau$). For both (a) and (b), there is an analogous graph where the photon is emitted off the positron leg. Both (b) and (c) only contribute to the amplitude when $\ell = e$.

their rest masses and their momentum is neglected in the Z and W propagators. To account for the bound state nature of Ps, we include p-Ps and o-Ps projection operators in the spinor trace of the amplitudes along with a factor of $\psi_0(0)/\sqrt{m}$ where $\psi_0(0)$ is the Ps ground state wave function. With these considerations, the Ps $\to \gamma\nu_\ell\bar{\nu}_\ell$ decay amplitudes are

$$\begin{aligned} i\mathcal{M}_{\mathrm{p/o}} &= -4\sqrt{2}ie\mathrm{G_F}m\frac{\psi_0(0)}{\sqrt{m}}\,\bar{u}(k_1)\gamma_\mu(v_\ell - a_\ell\gamma^5)v(k_2) \\ &\quad \times \mathrm{Tr}\,\Psi_{\mathrm{p/o}}\Bigg(\gamma^\mu\left(v_\ell - a_\ell\gamma^5\right)\frac{\not{p}_1 - \not{k}_\gamma + m}{(p_1 - k_\gamma)^2 - m^2}\not{\epsilon}^*_\gamma \\ &\quad + \not{\epsilon}^*_\gamma\frac{\not{k}_\gamma - \not{p}_2 + m}{(k_\gamma - p_2)^2 - m^2}\gamma^\mu\left(v_\ell - a_\ell\gamma^5\right)\Bigg) \end{aligned} \tag{2.1}$$

where $\mathrm{G_F} \simeq 1.166 \cdot 10^{-5}/\mathrm{GeV}^2$ is the Fermi constant [33], $\alpha \simeq 1/137$ is the fine structure constant, ϵ_γ is the photon polarization and $\Psi_{\mathrm{p/o}}$ are the p-Ps and o-Ps projection operators of Ref. [34]. Here, v_ℓ and a_ℓ describe the electron vector and axial-vector couplings induced by Z ($\ell = e, \mu, \tau$) and W ($\ell = e$; a Fierz transformation is understood [17])

boson exchange

$$v_\ell = \begin{cases} \frac{1}{4} + \sin^2\theta_{\rm W} & \text{for } \ell = e \\ \frac{1}{4} - \sin^2\theta_{\rm W} & \text{for } \ell = \mu, \tau, \end{cases} \tag{2.2}$$

$$a_\ell = \frac{1}{4}. \tag{2.3}$$

Since the weak mixing angle, θ_W, is such that $\sin^2\theta_{\rm W} \simeq 0.238$ [35] (numerically close to 1/4), the vector coupling is suppressed for $\ell = \mu, \tau$. We find the total decay rates

$$\Gamma_{\rm p} \equiv \Gamma(\text{p-Ps} \to \gamma\nu_\ell\bar{\nu}_\ell) = \frac{2{\rm G_F^2} m^5 \alpha^4 v_\ell^2}{9\pi^3} \approx \begin{cases} 3.5 \cdot 10^{-14}\ {\rm s}^{-1} & \text{for } \ell = e \\ 2.1 \cdot 10^{-17}\ {\rm s}^{-1} & \text{for } \ell = \mu, \tau, \end{cases} \tag{2.4}$$

$$\Gamma_{\rm o} \equiv \Gamma(\text{o-Ps} \to \gamma\nu_\ell\bar{\nu}_\ell) = \frac{8{\rm G_F^2} m^5 \alpha^4 a_\ell^2}{27\pi^3} \approx 1.2 \cdot 10^{-14}\ {\rm s}^{-1}. \tag{2.5}$$

The branching ratios are small, as expected for weak decays:

$$\text{Br}(\text{p-Ps} \to \gamma\nu\bar{\nu}) \approx \frac{\Gamma(\text{p-Ps} \to \gamma\nu_\ell\bar{\nu}_\ell)}{\Gamma(\text{p-Ps} \to 2\gamma)} \approx \begin{cases} 4.3 \cdot 10^{-24} & \text{for } \ell = e \\ 2.6 \cdot 10^{-27} & \text{for } \ell = \mu, \tau, \end{cases} \tag{2.6}$$

$$\text{Br}(\text{o-Ps} \to \gamma\nu\bar{\nu}) \approx \frac{\Gamma(\text{o-Ps} \to \gamma\nu_\ell\bar{\nu}_\ell)}{\Gamma(\text{o-Ps} \to 3\gamma)} \approx 1.7 \cdot 10^{-21} \text{ for } \ell = e, \mu, \tau. \tag{2.7}$$

We find that the o-Ps not only can decay radiatively into neutrinos, but also that since it can decay into all three flavors with equal probability, its total decay rate into $\nu\bar{\nu}\gamma$ is in fact slightly larger than for the p-Ps.

Equation (2.7) shows that the o-Ps branching ratio was overestimated by two orders of magnitude in [14]. The estimate of Ref. [14] has the correct powers of the universal constants, $\rm G_F, \alpha$, and m

$$\frac{\Gamma(\text{o-Ps} \to \gamma\nu_\ell\bar{\nu}_\ell)}{\Gamma(\text{o-Ps} \to 3\gamma)} \propto \left(\frac{{\rm G_F} m^2}{\alpha}\right)^2 \approx 10^{-19}. \tag{2.8}$$

However, the additional factor $4a_\ell^2/\left(3\pi^2(\pi^2-9)\right) \approx 0.01$ reduces the branching ratio by two orders of magnitude.

In Ref. [20], o-Ps is claimed not to decay into $\gamma\nu\bar{\nu}$, contrary to what we find. On the other hand, the decay rate of p-Ps into this final state seems to be overestimated by about a factor 60. Their result, presented as $\Gamma\left(\text{p-Ps} \to \gamma\nu_\ell\bar{\nu}_\ell\right) = \frac{\alpha^4 G_F^2 m^5}{\pi^3}\Sigma(\sin^2\theta_W)$, has the correct dependence on coupling constants and the mass, but the function of the weak mixing angle $\Sigma(\sin^2\theta_W)$ seems to be in error. This can be seen in equation (11) in [20] that describes the decay into muon neutrinos. Only the Z boson contributes in this channel, so the amplitude should be proportional to the vector coupling of the Z to electrons and vanish when $\sin^2\theta_W \to 1/4$; the expression in that equation does not vanish in this limit.

For the photon spectra we find very simple expressions,

$$\frac{1}{\Gamma_{\rm p}}\frac{{\rm d}\Gamma_{\rm p}}{{\rm d}x_\gamma} = 6x_\gamma(1-x_\gamma), \tag{2.9}$$

$$\frac{1}{\Gamma_{\rm o}}\frac{{\rm d}\Gamma_{\rm o}}{{\rm d}x_\gamma} = \frac{3}{2}x_\gamma(2-x_\gamma), \tag{2.10}$$

where $x_\gamma = E_\gamma/m \in (0,1)$. These spectra are shown in Fig. 2.2. Since there is some similarity between Ps $\to \gamma\nu_\ell\bar{\nu}_\ell$ and o-Ps $\to 3\gamma$ decays, the o-Ps $\to 3\gamma$ spectrum (first calculated by Ore and Powell [32]) is also included in Fig. 2.2 for comparison.

When the photon reaches the maximum energy, $x_\gamma = 1$, the neutrino (left-handed) and the antineutrino (right-handed) move collinearly in the direction opposite to the photon. Their spins cancel and the angular momentum of the system is carried by the photon's spin. Clearly, this is possible only for o-Ps; for this reason, the p-Ps spectrum vanishes at $x_\gamma = 1$ (Fig. 2.2(a)). This spectrum also vanishes at $x_\gamma = 0$. However, the p-Ps spectrum of Ref. [20] vanishes at neither $x_\gamma = 0$ or $x_\gamma = 1$.

The p-Ps spectrum is maximal at $x_\gamma = 1/2$; different from the maximum $x_\gamma = 2/3$, predicted in [20]. On the other hand the o-Ps spectrum is maximal at $x_\gamma = 1$ when the

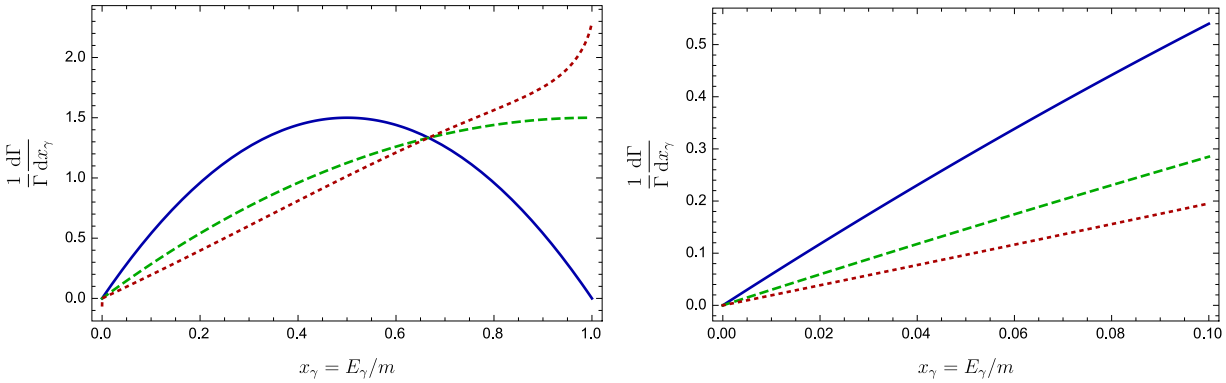

Figure 2.2: The photon spectrum of p-Ps $\to \gamma\nu_\ell\bar{\nu}_\ell$ (solid), o-Ps $\to \gamma\nu_\ell\bar{\nu}_\ell$ (dashed) and o-Ps $\to 3\gamma$ (dotted) decays plotted over (a) the full energy domain of the photon, $x_\gamma \in (0, 1)$ and (b) over the low-energy domain $x_\gamma \in (0, 0.1)$.

photon carries the whole angular momentum of the system.

We also note that the spectra we have found (neglecting binding effects) are linear in the low-energy limit (Fig. 2.2(b)). Since Low's theorem [25] predicts the low-energy behaviour of the spectrum to be cubic rather than linear, we shall determine how binding effects modify the results (2.9) and (2.10) (chapter 4).

Chapter 3

Angular distributions of Ps $\to \gamma\nu_\ell\bar{\nu}_\ell$ decays

In Chapter 2, we calculated the decay rates and spectra for p-Ps and o-Ps, and found that both can decay into a photon and a neutrino-antineutrino pair. To better understand these decays, we calculate the angular dependence of the Ps $\to \gamma\nu_\ell\bar{\nu}_\ell$ amplitudes (Sec. 3.1) and then use those amplitudes to determine the angular distributions of Ps $\to \gamma\nu_\ell\bar{\nu}_\ell$ decays (Sec. 3.2).

3.1 Angular dependence of the decay amplitudes

The angular dependence of the decay amplitudes is most easily found by reformulating the three-body decay Ps $\to \gamma\nu_\ell\bar{\nu}_\ell$ in terms of a two-body decay Ps $\to \gamma Z^*$, where Z^* is a fictitious massive vector boson of polarization ϵ and 4-momentum q. Specifically, the three-body phase space of the decay rate is factorized into two two-body phase spaces (one for Ps $\to \gamma Z^*$ and one for $Z^* \to \nu\bar{\nu}$) and an integral over the invariant mass squared of the Z^* boson (Appendix A). After integrating over the neutrino momenta, the Ps $\to \gamma\nu_\ell\bar{\nu}_\ell$ decay rate can be written as the integral of the Ps $\to \gamma Z^*$ decay rate (multiplied by a factor from the $Z^* \to \nu\bar{\nu}$ phase space) over the invariant mass of Z^*

squared (Appendix B),

$$\Gamma_{\text{p/o}} = \frac{\text{G}_\text{F}^2}{2\pi^2\alpha}\int \frac{\text{d}q^2}{2\pi} q^2 \Gamma_{\text{p/o-Ps}\to\gamma Z^*}, \tag{3.1}$$

where $q = k_1 + k_2$ is the Z^* 4-momentum and

$$\Gamma_{\text{p/o-Ps}\to\gamma Z^*} = \frac{1}{g}\frac{1}{2m_{\text{Ps}}}\int \text{d}\Phi_2\left(p_1+p_2; q, k_\gamma\right)\frac{|\psi_0(0)|^2}{m}\frac{1}{3}\sum_{\text{pol}}\left|\mathcal{M}_{\text{p/o-Ps}\to\gamma Z^*}\right|^2. \tag{3.2}$$

Here, g is the number of polarizations of the initial Ps state and the sum, $\sum_{\text{pol}}$, is over the Z^* polarizations.

From (3.1), it is clear that the three-body problem Ps $\to \gamma\nu_\ell\bar{\nu}_\ell$ can be described in terms of the two-body problem Ps $\to \gamma Z^*$. The Z^* couples to the electron current through both vector and axial-vector coupling with the Feynman rule $ie\not{\epsilon}^*\left(v_\ell - a_\ell\gamma^5\right)$ at each $e^+e^-Z^*$ vertex.

To construct the angular dependence of the Ps $\to \gamma Z^*$ decay amplitudes on the spherical angles θ and ϕ, we first determine the decay amplitudes to final states where the photon moves along the $+z$-axis and the Z^* boson moves along the $-z$-axis. The angular dependence is then determined by rotating the initial state and considering decay along the new z'-axis [36].

The p-Ps $\to \gamma Z^*$ decay amplitudes are isotropic and given by

$$\mathcal{A}_{m'_\gamma, m'_Z}(\theta,\phi) = B_{m'_\gamma, m'_Z} \propto \delta_{m'_\gamma, -m'_Z}, \tag{3.3}$$

where $m'_\gamma \in \{\pm 1\}$ and $m'_Z \in \{\pm 1, 0\}$ are the spin projections of the photon and Z^* along the z'-axis. The z'-axis points along the photon trajectory defined by the spherical polar angles θ and ϕ in the original unrotated frame. The p-Ps amplitudes along the z-axis, $B_{m'_\gamma, m'_Z}$, are calculated in Appendix C and the angular amplitudes, $\mathcal{A}_{m'_\gamma, m'_Z}(\theta,\phi)$, are listed in Table 3.1.

Table 3.1: The p-Ps $\to \gamma Z^*$ decay amplitudes, $\mathcal{A}_{m'_\gamma m'_Z}/v_\ell e^2$, as a function of the spherical angles θ and ϕ. Since p-Ps is odd under parity, $\mathcal{A}_{-m'_\gamma -m'_Z} = -\mathcal{A}_{m'_\gamma m'_Z}$; therefore, only the $m'_\gamma = +1$ amplitudes need be tabulated.

	m_{Z^*}		
m'_γ	$+1$	0	-1
$+1$	0	0	$4i/\sqrt{2}$

The o-Ps $\to \gamma Z^*$ amplitudes must be calculated for each initial polarization of o-Ps. In the initial frame before decay, the o-Ps atom is in a state of definite angular momentum with some spin projection along the z-axis. We let $|\Lambda\rangle$ represent this initial state. The o-Ps atom subsequently decays along the z'-axis with the amplitude $A_{m'_\gamma m'_Z}$ (Appendix C). Using the $A_{m'_\gamma m'_Z}$, the o-Ps angular amplitudes, $\mathcal{A}^{m_\Lambda}_{m'_\gamma m'_Z}$, are derived in Appendix D and are listed in Table 3.2. Here, $m_\Lambda \in \{\pm 1, 0\}$ is the initial spin projection of o-Ps along the z-axis.

Alternatively, one can obtain the angular dependence of the o-Ps $\to \gamma Z^*$ amplitudes using the helicity basis formalism (Appendix E).

Table 3.2: The o-Ps $\to \gamma Z^*$ decay amplitudes, $\mathcal{A}^{m_\Lambda}_{m'_\gamma m'_Z}/a_\ell e^2$, as a function of the spherical angles θ and ϕ evaluated at $\mathbf{q} = -\mathbf{k}_\gamma, E_Z = 2m - E_\gamma$. The $m_\Lambda = -1$ amplitudes can be obtained from the $m_\Lambda = +1$ amplitudes by the replacement $\theta \to \theta + \pi$ and $\phi \to -\phi$.

		m'_{Z^*}		
m_Λ	m'_γ	$+1$	0	-1
$+1$	$+1$	0	$\sqrt{2}(1+\cos\theta)e^{i\phi}/\sqrt{1-x_\gamma}$	$-2i\sin\theta e^{i\phi}$
	-1	$2i\sin\theta e^{i\phi}$	$-\sqrt{2}(1-\cos\theta)e^{i\phi}/\sqrt{1-x_\gamma}$	0
0	$+1$	0	$2\sin\theta/\sqrt{1-x_\gamma}$	$4i\cos\theta/\sqrt{2}$
	-1	$-4i\cos\theta/\sqrt{2}$	$-2\sin\theta/\sqrt{1-x_\gamma}$	0

To validate the amplitudes in Tables 3.1 and 3.2, we use them to calculate the decay rates and photon spectra, and compare these with those obtained in chapter 2. To do this, we first derive the spin averaged amplitudes squared. For p-Ps, this task is simple,

$$\frac{1}{3}\sum_{m'_\gamma m'_Z} \left|\mathcal{A}_{m_\gamma m'_Z}\right|^2_{\mathbf{q}=-\mathbf{k}_\gamma, E_Z = 2m - E_\gamma} = \frac{16 v_\ell^2 e^4}{3}. \tag{3.4}$$

To obtain the o-Ps spin averaged amplitude squared, it is convenient to first sum over m_Λ and m'_γ

$$\sum_{m_\Lambda m'_\gamma} \left|\mathcal{A}^{m_\Lambda}_{m_\gamma +}\right|^2_{\mathbf{q}=-\mathbf{k}_\gamma, E_Z=2m-E_\gamma} = \sum_{m_\Lambda m'_\gamma} \left|\mathcal{A}^{m_\Lambda}_{m_\gamma -}\right|^2_{\mathbf{q}=-\mathbf{k}_\gamma, E_Z=2m-E_\gamma} = 8a_\ell^2 e^4, \tag{3.5}$$

$$\sum_{m_\Lambda m'_\gamma} \left|\mathcal{A}^{m_\Lambda}_{m_\gamma 0}\right|^2_{\mathbf{q}=-\mathbf{k}_\gamma, E_Z=2m-E_\gamma} = \frac{16a_\ell^2 e^4}{1-x_\gamma}. \tag{3.6}$$

Then completing the sum over m'_Z and dividing by the number of o-Ps and Z^* polarizations yields the spin averaged amplitude squared

$$\begin{aligned}\frac{1}{3\cdot 3}\sum_{m_\Lambda m'_\gamma m'_Z} \left|\mathcal{A}^{m_\Lambda}_{m_\gamma m'_Z}\right|^2_{\mathbf{q}=-\mathbf{k}_\gamma, E_Z=2m-E_\gamma} &= \frac{2}{9}\left(8a_\ell^2 e^4\right) + \frac{16a_\ell^2 e^4}{9(1-x_\gamma)} \\ &= \frac{16a_\ell^2 e^4(2-x_\gamma)}{9(1-x_\gamma)}.\end{aligned} \tag{3.7}$$

Next, the Ps $\to \gamma Z^*$ decay rates are calculated by substituting equations (3.4) and (3.7) into (3.2). Since the spin averaged amplitudes squared are independent of angular location of the photon, θ_γ and ϕ_γ, the angular integrations in (3.2) are trivial

$$\begin{aligned}\Gamma_{\text{p/o-Ps}\to\gamma Z^*} &= \frac{1}{2m_{\text{Ps}}}\int \mathrm{d}\Phi_2\left(2p; q, k_\gamma\right)\frac{\left|\psi_0(0)\right|^2}{m}\frac{1}{3g}\sum_{\text{pol}}\left|\mathcal{M}_{\text{p/o-Ps}\to\gamma Z^*}\right|^2, \\ &= \frac{1}{2m_{\text{Ps}}}\frac{\tilde{\beta}(4m^2, q^2, 0)}{8\pi}\frac{\left|\psi_0(0)\right|^2}{m}\begin{Bmatrix} 16v_\ell^2 e^4/3 \\ 16a_\ell^2 e^4(2-x_\gamma)/9(1-x_\gamma)\end{Bmatrix} \\ &= \frac{\alpha^3 m^2}{3}\frac{4m^2-q^2}{4m^2}\begin{Bmatrix} v_\ell^2 \\ a_\ell^2(2-x_\gamma)/3(1-x_\gamma)\end{Bmatrix} \\ &= \frac{\alpha^3 m^2}{3}x_\gamma\begin{Bmatrix} v_\ell^2 \\ a_\ell^2(2-x_\gamma)/3(1-x_\gamma)\end{Bmatrix}\end{aligned} \tag{3.8}$$

where the top line in the curly brackets is used for the p-Ps (o-Ps) decay rate. Here, we have used equation (A.2) to simplify the two-body phase space in the second line and

$q^2 = 4m^2(1 - x_\gamma)$ to simplify the third line. Substituting the above equations into (3.1) and writing $\mathrm{d}q^2 = -4m^2\mathrm{d}x_\gamma$, we obtain the Ps $\to \gamma\nu_\ell\bar{\nu}_\ell$ photon spectrum and decay rates

$$\Gamma_{\mathrm{p/o}} = \frac{4\mathrm{G}_\mathrm{F}^2\alpha^4 m^5}{3\pi^3}\int_0^1 \mathrm{d}x_\gamma \begin{Bmatrix} v_\ell^2 x_\gamma(1-x_\gamma) \\ a_\ell^2 x_\gamma(2-x_\gamma)/3 \end{Bmatrix} \tag{3.9}$$

$$= \frac{4\mathrm{G}_\mathrm{F}^2\alpha^4 m^5}{9\pi^3}\begin{Bmatrix} v_\ell^2/2 \\ 2a_\ell^2/3 \end{Bmatrix}. \tag{3.10}$$

The decay rates (3.10) are identical to (2.4) and (2.5). The spectra are the integrands of equation (3.9) and are also equal to the spectra (2.9) and (2.10). Thus, the amplitudes of Tables 3.1 and 3.2 are consistent with our results from chapter 2.

While it is evident that p-Ps and o-Ps cannot decay into the same final states (even though they have the same constituent particles), we confirm the orthogonality of the p-Ps and o-Ps decay amplitudes. The o-Ps amplitudes, $\mathcal{A}^{m_\Lambda}_{\pm' 0'}$, are trivially orthogonal to the p-Ps amplitudes (3.3) because p-Ps cannot decay into a longitudinally polarized Z^* and photon. To check the orthogonality of $\mathcal{A}^{m_\Lambda}_{\pm' \mp'}$ with (3.3), we take their inner product

$$\int \mathrm{d}\Omega \mathcal{A}_{m_\gamma, m_Z}\left(\mathcal{A}^{m_\Lambda}_{\pm' \mp'}(\theta,\phi)\right)^* \propto \int \mathrm{d}\Omega \left(\mathcal{A}^{m_\Lambda}_{\pm' \mp'}(\theta,\phi)\right)^*. \tag{3.11}$$

Since $\mathcal{A}^{m_\Lambda}_{\pm' \mp'}(\theta,\phi)$ are proportional to $e^{\pm i\phi}$ or $\cos\theta$ (depending on m_Λ), the inner products vanish proving orthogonality; this is as expected because $\mathcal{A}^{m_\Lambda}_{\pm' \mp'}(\theta,\phi)$ (Table 3.2) are p-waves while the p-Ps amplitudes are s-waves (Table 3.1).

Thus, the p-Ps $\to \gamma\nu_\ell\bar{\nu}_\ell$ and o-Ps $\to \gamma\nu_\ell\bar{\nu}_\ell$ decays do not have access to the same final state although both the p-Ps and o-Ps final states contain the same constituent particles.

3.2 Angular distributions

The angular distribution for a specific $\gamma + Z^*$ final state is found by differentiating the decay amplitude (3.1) by x_γ and $\cos\theta$ where the squared amplitude corresponding to the specific final state (Tables 3.1 and 3.2) is used in place of the spin averaged amplitude squared.

Since the nonzero p-Ps amplitudes are isotropic, the nonzero p-Ps $\to \gamma\nu_\ell\bar{\nu}_\ell$ angular distributions are also isotropic

$$\frac{\mathrm{d}^2\Gamma_{m'_\gamma=\pm';m'_Z=\mp'}}{\mathrm{d}x_\gamma \mathrm{d}\cos\theta} = \frac{9\Gamma_\mathrm{p} x_\gamma(1-x_\gamma)}{2}. \tag{3.12}$$

Thus, p-Ps is equally likely to decay into a photon and a neutrino-antineutrino pair where the photon is emitted in any direction.

The o-Ps $\to \gamma\nu_\ell\bar{\nu}_\ell$ angular distributions are determined to be

$$\frac{1}{\Gamma_\mathrm{o}}\frac{\mathrm{d}^2\Gamma^{m_\Lambda}_{m'_\gamma m'_Z}}{\mathrm{d}x_\gamma \mathrm{d}\cos\theta} = \frac{27}{64}x_\gamma(1-x_\gamma)\int\frac{\mathrm{d}\phi}{2\pi}\left|\frac{\mathcal{A}^{m_\Lambda}_{m'_\gamma m'_Z}}{a_\ell e^2}\right|^2_{\mathbf{q}=-\mathbf{k}_\gamma, E_Z=2m-E_\gamma} \tag{3.13}$$

and are tabulated in Table 3.3. Since Z^* is a mathematical convenience, the physical angular distribution for a given o-Ps polarization m_Λ and photon helicity m'_γ is obtained by averaging over the Z^* polarizations. For an o-Ps atom initially polarized in the $m_\Lambda = 0$

Table 3.3: Angular distributions of o-Ps $\to \gamma\nu_\ell\bar{\nu}_\ell$ decays, $(\mathrm{d}^2\Gamma^{m_\Lambda}_{m'_\gamma m'_Z}/\mathrm{d}x_\gamma\mathrm{d}\cos\theta)/\Gamma_\mathrm{o}$. The $m_\Lambda = -1$ distributions can be obtained from the $m_\Lambda = +1$ angular distributions by the replacement $\theta \to \theta + \pi$ and $\phi \to -\phi$.

		m'_{Z^*}		
m_Λ	m'_γ	$+1$	0	-1
$+1$	$+1$	0	$27\cos^4(\theta/2)x_\gamma/8$	$27\sin^2\theta x_\gamma(1-x_\gamma)/16$
	-1	$27\sin^2\theta x_\gamma(1-x_\gamma)/16$	$27\sin^4(\theta/2)x_\gamma/8$	0
0	$+1$	0	$27\sin^2\theta x_\gamma/16$	$27\cos^2\theta x_\gamma(1-x_\gamma)/8$
	-1	$27\cos^2\theta x_\gamma(1-x_\gamma)/8$	$27\sin^2\theta x_\gamma/16$	0

state, the angular distributions for decay into a photon of helicity $m'_\gamma = \pm 1$ are

$$\frac{1}{3}\sum_{m'_Z}\frac{\mathrm{d}^2\Gamma^0_{\pm' m'_Z}}{\mathrm{d}x_\gamma \mathrm{d}\cos\theta} = \frac{9}{16}\Gamma_{\mathrm{o}} x_\gamma \left[\sin^2\theta + 2\cos^2\theta(1-x_\gamma)\right], \tag{3.14}$$

which are non-zero for all θ. The angular distribution for o-Ps initially polarized in the $m_\Lambda = +1$ state decaying into a photon of helicity $m'_\gamma = +1$ is

$$\frac{1}{3}\sum_{m'_Z}\frac{\mathrm{d}^2\Gamma^+_{+' m'_Z}}{\mathrm{d}x_\gamma \mathrm{d}\cos\theta} = \frac{9}{16}\Gamma_{\mathrm{o}} x_\gamma \left[2\cos^4(\theta/2) + \sin^2\theta(1-x_\gamma)\right]. \tag{3.15}$$

Since this angular distribution vanishes for $\theta = \pi$, an o-Ps atom in the $m_\Lambda = +1$ state cannot decay into a photon of helicity $m'_\gamma = +1$ along the $-z$-axis. Similarly, an o-Ps atom initially polarized in the $m_\Lambda = +1$ state cannot decay into a photon of helicity $m'_\gamma = -1$ along the $+z$-axis.

The photon spectrum for a specific $\gamma + Z^*$ final state is calculated by integrating the corresponding angular distribution by $\mathrm{d}\cos\theta$. These spectra are listed in Tables 3.4 and 3.5 and provide further insight into equations (2.9) and (2.10).

Table 3.4: p-Ps $\to \gamma\nu_\ell\bar{\nu}_\ell$ photon spectra, $(\mathrm{d}\Gamma_{m'_\gamma m'_Z}/\mathrm{d}x_\gamma)/\Gamma_{\mathrm{p}}$, for specific $\gamma + Z^*$ final states. Since $|\mathcal{A}_{m'_\gamma m'_Z}|^2 = |\mathcal{A}_{-m'_\gamma -m'_Z}|^2$, only the $m'_\gamma = +1$ decay rates need be tabulated.

	m'_{Z^*}		
m'_γ	$+1$	0	-1
$+1$	0	0	$9x_\gamma(1-x_\gamma)$

Table 3.5: o-Ps $\to \gamma\nu_\ell\bar{\nu}_\ell$ photon spectra, $(\mathrm{d}\Gamma^{m_\Lambda}_{m'_\gamma m'_Z}/\mathrm{d}x_\gamma)/\Gamma_{\mathrm{o}}$, for specific $\gamma + Z^*$ final states and any m_Λ.

	m'_{Z^*}		
m'_γ	$+1$	0	-1
$+1$	0	$9x_\gamma\ /4$	$9x_\gamma(1-x_\gamma)/4$
-1	$9x_\gamma(1-x_\gamma)/4$	$9x_\gamma/4$	0

From Tables 3.4 and 3.5, we see that the nonzero photon spectra of decays into final states with $m'_\gamma = \pm 1$ and $m'_Z = \mp 1$ are proportional to $x_\gamma\,(1 - x_\gamma)$ and vanish as $x_\gamma \to 1$. On the other hand, the nonzero photon spectra of decays into final states with $m'_\gamma = \pm 1$ and $m'_Z = 0$ are linear and maximal at $x_\gamma \to 1$.

The o-Ps photon spectrum is maximal at $x_\gamma = 1$ because the o-Ps decay has access to two final states with a longitudinally polarized Z^*, which add to the linear term in the spectrum, unlike the p-Ps decay. Specifically, the $\mathcal{A}^{m_\Lambda}_{\pm 0}$ amplitudes contain a factor of $2m/q = 1/\sqrt{1 - x_\gamma}$ from the longitudinal polarization of Z^* that enhances the amplitude for high-energy photons and when squared cancels the factor $q^2 \propto (1 - x_\gamma)$ in the $\mathrm{d}q^2$ integral of (3.1). Physically, the high-energy limit $x_\gamma \to 1$, the longitudinal polarization of Z^* represents a final state where the neutrino and antineutrino are collinear.

Lastly, we note that the photon spectra (2.9) and (2.10) can be obtained from Tables 3.4 and 3.5 by averaging over the photon and Z^* polarizations and summing over the photon polarizations

$$\frac{1}{3} \sum_{m'_\gamma m'_Z} \frac{\mathrm{d}\Gamma_{m'_\gamma m'_Z}}{\mathrm{d}x_\gamma} = 6\Gamma_{\mathrm{p}} x_\gamma (1 - x_\gamma), \tag{3.16}$$

$$\frac{1}{9} \sum_{m_\Lambda m'_\gamma m'_Z} \frac{\mathrm{d}\Gamma^{m_\Lambda}_{m'_\gamma m'_Z}}{\mathrm{d}x_\gamma} = \frac{3\Gamma_{\mathrm{o}}}{2} x_\gamma (1 - x_\gamma). \tag{3.17}$$

It is clear that the decay rates (2.4) and (2.5) are obtained by integrating the above over x_γ.

Chapter 4

Low's theorem and the soft photon limit of the spectra

Low's theorem [25] places constraints on the amplitude of any radiative process and predicts the spectrum in the soft photon limit. In chapter 2, the tree level electroweak photon spectra, equations (2.9) and (2.10), were found to be linear in the low-energy limit, similar to the Ore-Powell o-Ps $\to 3\gamma$ spectrum [32]. However, it was pointed out by Ref. [21] that the Ore-Powell spectrum is in contradiction with Low's theorem. Therefore, it is important to reconcile any discrepancy between Low's theorem and equations (2.9) and (2.10).

Low's theorem states that the $\mathcal{O}(E_\gamma^{-1})$ and $\mathcal{O}(E_\gamma^0)$ terms in the Laurent expansion of the radiative amplitude, $X \to Y + \gamma$, are obtained from knowledge of the non-radiative amplitude, $X \to Y$ [21, 22, 25]. Expanding the radiative amplitude, $\epsilon_\gamma^\mu \mathcal{M}_\mu$, in a Laurent series in the photon energy, we obtain

$$\epsilon_\gamma^\mu \mathcal{M}_\mu = \sum_{n=-1}^{\infty} \mathcal{M}_{n+1} E_\gamma^n, \tag{4.1}$$

where $\mathcal{M}_i$ is the coefficient of the $\mathcal{O}\left(E_\gamma^i\right)$ term of the Laurent series. The coefficients

$\mathcal{M}_0$ and $\mathcal{M}_1$ are independent of E_γ and determined by the non-radiative amplitude, its derivatives in physically allowed regions and the anomalous magnetic moments of the particles involved in the reaction [25].

The $\mathcal{M}_0$ coefficient is proportional to the non-radiative amplitude multiplied by the factor $-Q_i\epsilon \cdot p_i/k_\gamma \cdot p_i$, which arises from the emission of a photon by an outgoing or ingoing particle [22]. The $\mathcal{M}_0$ coefficient vanishes when there are no moving charged particles in the initial and final state of the non-radiative process or when the non-radiative amplitude is zero. The coefficient $\mathcal{M}_1$ is a function of the magnetic moments of the particles as well as the non-radiative amplitude and its derivatives with respect to energy and angle [25].

By combining the behavior of the radiative amplitude and the phase space, we find that the low-energy photon spectrum has the form

$$\frac{\mathrm{d}\Gamma}{\mathrm{d}E_\gamma} = \frac{A}{E_\gamma} + B + CE_\gamma + DE_\gamma^2 + \mathcal{O}\left(E_\gamma^3\right), \tag{4.2}$$

where

$$\begin{aligned} A &= |\mathcal{M}_0|^2 \\ B &= \mathcal{M}_0\mathcal{M}_1^* + \mathcal{M}_1\mathcal{M}_0^* \\ C &= |\mathcal{M}_1|^2 + \mathcal{M}_0\mathcal{M}_2^* + \mathcal{M}_2\mathcal{M}_0^* \\ D &= \mathcal{M}_0\mathcal{M}_3^* + \mathcal{M}_3\mathcal{M}_0^* + \mathcal{M}_1\mathcal{M}_2^* + \mathcal{M}_2\mathcal{M}_1^*. \end{aligned} \tag{4.3}$$

If $\mathcal{M}_0$ vanishes, then $A = B = 0$ and the soft photon spectrum is of order $E_\gamma \mathrm{d}E_\gamma$. If both $\mathcal{M}_0$ and $\mathcal{M}_1$ vanish, then $A = B = C = D = 0$ and the soft photon spectrum is of order $E_\gamma^3 \mathrm{d}E_\gamma$.

For p-Ps $\to \gamma\nu_\ell\bar{\nu}_\ell$, the non-radiative p-Ps $\to \nu_\ell\bar{\nu}_\ell$ amplitude vanishes [17]; application of Low's theorem yields $\mathcal{M}_{0,1} = 0$ for the radiative decay, p-Ps $\to \gamma\nu_\ell\bar{\nu}_\ell$. Since the

radiative o-Ps $\to \gamma\nu_\ell\bar{\nu}_\ell$ decay proceeds only via axial-vector coupling while the non-radiative o-Ps $\to \nu_\ell\bar{\nu}_\ell$ amplitude is proportional to vector coupling [17], Low's theorem requires the $\mathcal{O}(E_\gamma^{-1})$ and $\mathcal{O}(E_\gamma^0)$ terms of the radiative o-Ps $\to \gamma\nu_\ell\bar{\nu}_\ell$ amplitude to vanish (*i.e.*, $\mathcal{M}_{0,1} = 0$). Thus, for both Ps $\to \gamma\nu_\ell\bar{\nu}_\ell$ decays, Low's theorem predicts that the photon spectra are cubic in the low-energy limit in apparent contradiction with equations (2.9) and (2.10).

Equations (2.9) and (2.10) were calculated using the tree level electroweak amplitude for the $e^+e^- \to \gamma\nu_\ell\bar{\nu}_\ell$ annihilation multiplied by the probability density for the e^+e^- pair to be at the origin. This calculation assumes that the electron and positron are initially free and at rest, and therefore neglects the binding effects in Ps (which are of order $m\alpha^2$). For photons with comparable energies, binding effects become important and equations (2.9) and (2.10) are no longer accurate.

To resolve the contradiction between equations (2.9) and (2.10), and Low's theorem, we must include binding effects in the soft photon spectrum of Ps $\to \gamma\nu_\ell\bar{\nu}_\ell$ decays. To do this we employ the non-relativistic effective field theory (NREFT) methods developed in Refs. [22, 24, 23].

Chapter 5

Soft photon spectra of Ps $\to \gamma\nu_\ell\bar{\nu}_\ell$ decays

NREFTs provide a systematic way of incorporating binding effects in the computation of bound state decay amplitudes. One computes the decay amplitudes in electroweak theory. Then a NREFT Hamiltonian is constructed to reproduce the soft photon limit of the electroweak amplitudes when ignoring binding effects. In other words, the effective theory dynamics (ignoring binding effects) are set equal to the low-energy limit of the electroweak dynamics.

Once this matching has been performed, the NREFT Hamiltonian is used to calculate the effective theory amplitudes and subsequently the soft photon spectra. The effective theory amplitudes are calculated using time-independent perturbation theory and have both long (Coulomb) and short distance (annihilation into a $\nu_\ell\bar{\nu}_\ell$ pair) contributions.

We calculate the soft-photon limit of the Ps $\to \gamma\nu_\ell\bar{\nu}_\ell$ electroweak amplitudes in Sec. 5.1. The matching conditions and effective theory photon spectra are calculated in Secs. 5.3 and 5.4.

The Coulomb (H_C) and the interaction ($H_{\rm int}$) Hamiltonians describe the bound state dynamics of an e^+e^- pair interacting with a quantized electromagnetic field. Following

Ref. [23], we argue that the dipole approximation of the interaction Hamiltonian is valid in the energy range $E_\gamma \ll m$ (Sec. 5.2). In the dipole approximation, the Hamiltonians are

$$
\begin{aligned}
H &= H_{\rm C} + H_{\rm int}, && (5.1)\\
H_{\rm C} &= \frac{\mathbf{p}^2}{m} - \frac{\alpha}{r}, && (5.2)\\
H_{\rm int} &= -e\mathbf{x}\cdot\mathbf{E} - \mu\left[\boldsymbol{\sigma}_\phi + \boldsymbol{\sigma}_\chi\right]\cdot\mathbf{B}, && (5.3)
\end{aligned}
$$

in terms of the center of mass variables $\mathbf{p} = (\mathbf{p}_1 - \mathbf{p}_2)/2$ and $\mathbf{x} = \mathbf{x}_1 - \mathbf{x}_2$ where the indices 1 and 2 refer to the electron and positron [22]. Here, $\boldsymbol{\sigma}_{\phi/\chi}$ are the Pauli matrices acting on the electron (ϕ) and positron (χ) Pauli spinors. The electric, $\mathbf{E}$, and magnetic, $\mathbf{B}$, fields are evaluated in the dipole approximation. Therefore, $H_{\rm int}$ can induce both E1 and M1 transitions within the Ps atom.

The Coulomb Hamiltonian H_C is the leading term in the velocity, $v \ll 1$, of the electron. The interaction Hamiltonian, $H_{\rm int}$, is higher order in v and taken as a perturbation. The (p/o)-Ps annihilation amplitude is given by the first order v expansion of the electroweak $e^+e^- \to \nu_\ell\bar{\nu}_\ell$ annihilation amplitude. While the neutrino energies are of order $\mathcal{O}(m)$, a non-relativistic treatment is still valid since the annihilation into a neutrino-antineutrino pair is a short distance effect – the neutrinos are not dynamical.

5.1 Soft photon limit of the tree level electroweak decay amplitude

Using the standard Feynman rules, the Ps $\to \gamma\nu\bar{\nu}$ decay amplitude (Fig. 2) is

$$\mathcal{M} = -2\sqrt{2}i\mathrm{G_F}em\bar{v}\left(p_2\right)\left(\not{J}\left(v_\ell - a_\ell\gamma^5\right)\frac{\not{p}_1 - \not{k}_\gamma + m}{(p_1 - k_\gamma)^2 - m^2}\not{\epsilon}^*_\gamma + \not{\epsilon}^*_\gamma\frac{\not{k}_\gamma - \not{p}_2 + m}{(k_\gamma - p_2)^2 - m^2}\not{J}\left(v_\ell - a_\ell\gamma^5\right)\right)u\left(p_1\right), \quad (5.4)$$

where p_1 and p_2 are the electron and positron 4-momenta, k_1 and k_2 are the neutrino and antineutrino 4-momenta, k_γ is the photon 4-momentum and ϵ_γ is the photon polarization. Here, $J^\mu\left(k_1, k_2\right) = \bar{u}(k_1)\gamma^\mu\left(1 - \gamma^5\right)v(k_2)$ is the neutral weak current (see equation (F.6) in Appendix F).

In equation (5.4), we choose the Dirac representation of the gamma matrices and Dirac spinors for the electron and positron. In this representation, the electron spinor is

$$u_s(p) = \frac{1}{\sqrt{E+m}}\begin{pmatrix} E+m \\ \mathbf{p}\cdot\boldsymbol{\sigma} \end{pmatrix}\phi_s, \quad (5.5)$$

where $E = \sqrt{m^2 + \mathbf{p}^2}$, ϕ_s is the two-component electron spinor and the index s denotes the spin projection [37]. The positron spinors are related to the electron spinors by charge conjugation,

$$v_s\left(p\right) = \frac{1}{\sqrt{E+m}}\begin{pmatrix} \mathbf{p}\cdot\boldsymbol{\sigma} \\ E+m \end{pmatrix}\chi_s, \quad (5.6)$$

where $\chi_s = i\sigma^2\phi^*_s$ is the two-component positron spinor.

Since the Ps binding energy is small, $\mathcal{O}(m\alpha^2)$, the typical momentum of the electron is small and we neglect it (i.e., $p_1 = p_2 = (m, \mathbf{0})$). In the limit $E_\gamma \to 0$, the neutrino momenta are back to back ($\mathbf{k}_1 = -\mathbf{k}_2$) and $J^0 \to 0$. Factoring out the E_γ dependence

and working with $\hat{\mathbf{k}}_\gamma = \mathbf{k}_\gamma/E_\gamma$, equation (5.4) becomes

$$\mathcal{M} = 2\sqrt{2}\mathrm{G_F} e\chi^\dagger \left(v_\ell \left(\hat{\mathbf{k}}_\gamma \times \boldsymbol{\epsilon}_\gamma \right) \cdot \mathbf{J} + a_\ell \left(\boldsymbol{\epsilon}_\gamma \times \mathbf{J} \right) \cdot \boldsymbol{\sigma} \right) \phi, \tag{5.7}$$

where we choose ϵ_γ to be real and transverse to k_γ. Projecting the electron and positron spinors onto the p-Ps ($\chi^\dagger\phi \to \sqrt{2}$ and $\chi^\dagger\boldsymbol{\sigma}\phi \to \mathbf{0}$) and o-Ps ($\chi^\dagger\phi \to 0$ and $\chi^\dagger\boldsymbol{\sigma}\phi \to \sqrt{2}\boldsymbol{\xi}$) states, the low-energy limit of the electroweak amplitudes are

$$\mathcal{M}_\mathrm{p} = 4\mathrm{G_F} e v_\ell \left(\boldsymbol{\epsilon}_\gamma \times \mathbf{J} \right) \cdot \hat{\mathbf{k}}_\gamma, \tag{5.8}$$

$$\mathcal{M}_\mathrm{o} = 4\mathrm{G_F} e a_\ell \left(\boldsymbol{\epsilon}_\gamma \times \mathbf{J} \right) \cdot \boldsymbol{\xi}, \tag{5.9}$$

where $\boldsymbol{\xi}$ is the o-Ps polarization vector.

5.2 Dipole approximation of the interaction Hamiltonian

While normally the dipole approximation is applicable for photons with wavelengths much larger than the spatial extent of the Ps atom, $2/m\alpha$ (i.e., $E_\gamma \ll m\alpha$), it has been shown that the dipole approximation of the interaction Hamiltonian holds in the enlarged energy region $E_\gamma \ll m$ for the three-body decay o-Ps $\to 3\gamma$ [23, 24]. In this energy region, amplitudes where the intermediate states propagate via the Coulomb Green's function, are a series in $\alpha\sqrt{m/E_\gamma} \sim \sqrt{\alpha}$ rather than integer powers of α. The main contributions to the effective field theory amplitudes arise from distances of order $\mathcal{O}(1/\sqrt{mE_\gamma})$, which are much smaller than the Ps radius $\mathcal{O}(1/m\alpha)$ [24]. We argue that the same considerations apply to Ps $\to \gamma\nu_\ell\bar{\nu}_\ell$ decays and that the dipole approximation holds in the extended energy range $E_\gamma \ll m$.

Initially, the Ps atom is in either the ${}^1S_0$ or ${}^3S_1$ states at energy $E_1 = -m\alpha^2/4$

relative to the threshold. The p-Ps (o-Ps) atom then emits a soft photon and the e^+e^- pair propagates non-relativistically in the Coulomb field in a C-odd (C-even) state of energy $E_1 - E_\gamma$ before annihilating into a neutrino-antineutrino pair (Fig. 5.1).

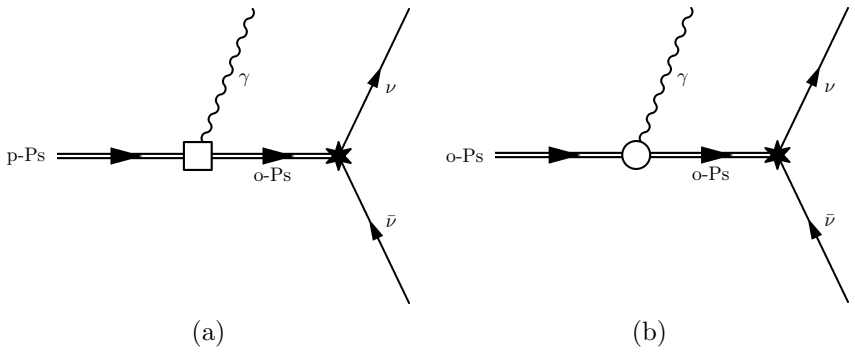

Figure 5.1: Effective theory graphs for (a) p-Ps $\to \gamma\nu_\ell\bar{\nu}_\ell$ and (b) o-Ps $\to \gamma\nu_\ell\bar{\nu}_\ell$. The open square (circle) represents a M1 (E1) transition while the solid star represents the annihilation of o-Ps into a neutrino-antineutrino pair.

The Green's function of the e^+e^- pair, interacting via a Coulomb field, G_C, describes the propagation of the pair between the emission of the soft photon and the annihilation into a neutrino-antineutrino pair. It satisfies the equation

$$\left(H_C + \frac{\kappa^2}{m}\right) G_C(\mathbf{x}, \mathbf{y}; \kappa) = \delta\left(\mathbf{x} - \mathbf{y}\right) \tag{5.10}$$

and is proportional to $\exp\left(-\kappa r\right)$ where $-\kappa^2/m = E_\gamma$. Therefore, the virtual pair propagates over a distance of $\mathcal{O}(\kappa^{-1})$ [23].

Since the spin-singlet state cannot annihilate into a neutrino-antineutrino pair [17], the virtual C-odd (C-even) state of Fig. 5.1(a) (5.1(b)) must be a triplet state of orbital angular momentum $L = 2n$ ($L = 2n + 1$) for n a non-negative integer. The transition amplitude for ${}^1S \to {}^3(2n) + \gamma$ (${}^3S \to {}^3(2n + 1) + \gamma$) is a magnetic M($2n$) (electric E($2n + 1$)) type interaction and proportional to $(E_\gamma/m)(E_\gamma r)^{2n}$ ($(E_\gamma r)^{2n+1}$). Furthermore, the amplitude for annihilation contains L derivatives of the Green's function and is proportional to $(\kappa/m)^L$. Since the exponential dependence of the Green's function, $\exp(-\kappa r)$, constrains the product κr to order one, the total amplitude scales with the

photon energy as $(E_\gamma/m)^{2n+1}$ [23].

Therefore, only the intermediate states with the lowest n (i.e., $n = 0$) need to be considered for $E_\gamma \ll m$ [23]. The intermediate state of Fig. 5.1(a) is the o-Ps ground state, 1^3S_1, while the intermediate states of Fig. 5.1b are the $L = 1$ o-Ps excited states, $n^3P_{0,1,2}$. These states are reached from the initial p-Ps and o-Ps ground states by M1 and E1 transitions respectively. Thus, the dipole approximation is valid in the energy region $E_\gamma \ll m$.

5.3 Soft photon spectrum for p-Ps

As noted in Sec. 5.2, p-Ps cannot decay into a $\nu_\ell\bar{\nu}_\ell$ pair; therefore, the p-Ps $\to \gamma\nu_\ell\bar{\nu}_\ell$ decay must proceed solely through an M1 transition. The M1 interaction flips the spin of either the electron or positron and takes the initial p-Ps state, 1^1S_0, to an intermediate o-Ps state. Within the dipole approximation, the only allowed intermediate state is the o-Ps ground state, 1^3S_1.

In time-ordered perturbation theory, the effective theory amplitude for p-Ps $\to \gamma\nu_\ell\bar{\nu}_\ell$, Fig. 5.1(a), is

$$\begin{aligned}\mathcal{M}_{\rm p}^{\rm eff} &= \sum_n \frac{i\langle 0|\hat{A}_{\rm s}^{(\nu_\ell\bar{\nu}_\ell)}|n\rangle\langle n|i\mu\,(\boldsymbol{\sigma}_\phi+\boldsymbol{\sigma}_\chi)\cdot\mathbf{B}|\text{p-Ps}\rangle}{E_{\rm p}-E_n-E_\gamma} \\ &= \sum_{m_s} \frac{-i\langle 0|\hat{A}_{\rm s}^{(\nu_\ell\bar{\nu}_\ell)}|1^3S_1;m_s\rangle\langle 1^3S_1;m_s|i\mu\,(\boldsymbol{\sigma}_\phi+\boldsymbol{\sigma}_\chi)\cdot\mathbf{B}|\text{p-Ps}\rangle}{\Delta E_{\rm hfs}+E_\gamma}, \qquad (5.11)\end{aligned}$$

where $\Delta E_{\rm hfs} = E_{\rm o} - E_{\rm p}$ is the hyperfine splitting energy difference, and, $E_{\rm p}$ and $E_{\rm o}$ are the p-Ps and o-Ps ground state energies. Here, $\hat{A}_{\rm s}^{(\nu_\ell\bar{\nu}_\ell)}$ is the s-wave o-Ps $\to \nu_\ell\bar{\nu}_\ell$ annihilation operator (Appendix G),

$$\hat{A}_{\rm s}^{(\nu_\ell\bar{\nu}_\ell)} = 2\sqrt{2}i\mathrm{G_F}mv_\ell\,(\mathbf{J}\cdot\boldsymbol{\sigma})\,. \qquad (5.12)$$

To simplify the effective theory amplitude, we begin by evaluating the annihilation and magnetic matrix elements in the numerator. Projecting the electron and positron spinors

onto the spin triplet state ($\chi^\dagger \boldsymbol{\sigma}\phi \to \sqrt{2}\boldsymbol{\xi}$), the annihilation matrix element becomes

$$\begin{aligned}\langle 0|\hat{A}_{\rm s}^{(\nu_\ell\bar{\nu}_\ell)}|1^3S_1;m_s\rangle &= 2\sqrt{2}i{\rm G_F}mv_\ell\mathbf{J}\cdot\left(\chi^\dagger\boldsymbol{\sigma}\phi\right)\psi_0(0)\\ &= 4i{\rm G_F}mv_\ell\mathbf{J}\cdot\boldsymbol{\xi}\psi_0(0),\end{aligned} \tag{5.13}$$

where ψ_0 is the Ps ground state wave function. The magnetic matrix element is

$$\begin{aligned}\langle 1^3S_1;m_s|i\mu\left(\boldsymbol{\sigma}_\phi+\boldsymbol{\sigma}_\chi\right)\cdot\mathbf{B}|\text{p-Ps}\rangle &= \frac{e}{\sqrt{2}m}E_\gamma\left(\hat{\mathbf{k}}_\gamma\times\boldsymbol{\epsilon}_\gamma\right)\cdot\left(\chi^\dagger\boldsymbol{\sigma}\phi\right)^*\\ &= \frac{e}{\sqrt{2}m}E_\gamma\left(\hat{\mathbf{k}}_\gamma\times\boldsymbol{\epsilon}_\gamma\right)\cdot\sqrt{2}\boldsymbol{\xi}^*.\end{aligned} \tag{5.14}$$

Summed over the polarizations of the intermediate o-Ps states in (5.11),

$$\sum_{\boldsymbol{\xi}}\boldsymbol{\xi}^i\boldsymbol{\xi}^{i*}=\delta^{ij}, \tag{5.15}$$

the effective theory amplitude becomes

$$\mathcal{M}_{\rm p}^{\rm eff} = 4{\rm G_F}ev_\ell\,\psi_0(0)\left(\boldsymbol{\epsilon}_\gamma\times\mathbf{J}\right)\cdot\hat{\mathbf{k}}_\gamma\,\mathcal{A}_{\rm m}(E_\gamma). \tag{5.16}$$

The magnetic amplitude, $\mathcal{A}_{\rm m}$, contains all the dependence on the soft photon energy in the effective theory amplitude,

$$\mathcal{A}_{\rm m}(E_\gamma)=\frac{E_\gamma}{\Delta E_{\rm hfs}+E_\gamma}=\frac{x_\gamma}{\epsilon+x_\gamma},\quad \epsilon\equiv\frac{\Delta E_{\rm hfs}}{m}. \tag{5.17}$$

To ensure that the effective theory amplitude (5.16) is consistent with electroweak theory, we consider $x_\gamma \gg \epsilon$ and neglect the hyperfine energy difference in the energy denominator of (5.11); then, $\mathcal{A}_m = 1$. The effective theory amplitude, ignoring binding effects, is therefore

$$\mathcal{M}_{\rm p}^{\rm eff}\to 4{\rm G_F}ev_\ell\,\psi_0(0)\left(\boldsymbol{\epsilon}_\gamma\times\mathbf{J}\right)\cdot\hat{\mathbf{k}}_\gamma. \tag{5.18}$$

Since (5.18) is equal to the soft photon limit of the tree level electroweak amplitude (5.8)[1], the annihilation operator (5.12) and M1 transition fully account for $\nu_\ell\bar{\nu}_\ell$ annihilation and soft photon emission in p-Ps $\to \gamma\nu_\ell\bar{\nu}_\ell$ decays.

Assured that the effective theory amplitude (5.16) is consistent with the full electroweak theory, we use it to calculate the low-energy photon spectrum. We need both the three body phase space in the $x_\gamma \to 0$ limit and the spin averaged amplitude squared. In the $x_\gamma \to 0$ limit, the three body phase space is

$$\left[\frac{1}{128\pi^3}\mathrm{d}x_1\mathrm{d}x_\gamma\right]_{x_\gamma\to 0} \approx \frac{1}{128\pi^3}\frac{x_\gamma}{2}\mathrm{d}\cos\theta\mathrm{d}x_\gamma, \tag{5.19}$$

where θ is the angle between the neutrino and photon. The spin averaged square of the amplitude is

$$\begin{aligned}\sum_{\boldsymbol{\epsilon}_\gamma}\left|\mathcal{M}_{\mathrm{p}}^{\mathrm{eff}}\right|^2 &= \sum_{\boldsymbol{\epsilon}_\gamma}\left|4\mathrm{G_F}ev_\ell\psi_0(0)\mathcal{A}_{\mathrm{m}}(E_\gamma)\left(\boldsymbol{\epsilon}_\gamma\times\mathbf{J}\right)\cdot\hat{\mathbf{k}}_\gamma\right|^2 \\ &\underset{x_\gamma\to 0}{\longrightarrow} 128\mathrm{G_F^2}v_\ell^2\alpha^4m^5\left|\mathcal{A}_{\mathrm{m}}(E_\gamma)\right|^2\left(1+\cos^2\theta\right),\end{aligned} \tag{5.20}$$

where $\sum_{\boldsymbol{\epsilon}_\gamma}\left|\left(\boldsymbol{\epsilon}_\gamma\times\mathbf{J}\right)\cdot\hat{\mathbf{k}}_\gamma\right|^2 = 16E_1^2\left[1+(\hat{\mathbf{k}}_\gamma\cdot\hat{\mathbf{k}}_1)^2\right]$ (see equation (F.15) in Appendix F), $\hat{\mathbf{k}}_\gamma\cdot\hat{\mathbf{k}}_1 = \cos\theta$ and $E_1 \to m$. Here, $\hat{\mathbf{k}}_1$ and $\hat{\mathbf{k}}_\gamma$ are the unit 3-momentum vectors of the neutrino and photon.

The effective theory photon spectrum is obtained by multiplying (5.20) by (5.19) and integrating over $\mathrm{d}\cos\theta$ where the allowed integration range is $-1 \le \cos\theta \le 1$

$$\begin{aligned}\left(\frac{1}{\Gamma_{\mathrm{p}}}\frac{\mathrm{d}\Gamma_{\mathrm{p}}}{\mathrm{d}x_\gamma}\right)^{\mathrm{eff}} &= \frac{9\pi^3}{2m^5\alpha^4\mathrm{G_F^2}v_\ell^2}\int_{-1}^{1}\mathrm{d}\cos\theta\frac{1}{128\pi^3}\frac{x_\gamma}{2}\sum_{\boldsymbol{\epsilon}_\gamma}\left|\mathcal{M}_{\mathrm{p}}^{\mathrm{eff}}\right|^2 \\ &= 6x_\gamma\left|\mathcal{A}_{\mathrm{m}}(E_\gamma)\right|^2.\end{aligned} \tag{5.21}$$

The spectrum is proportional to the square of the magnetic amplitude, $\mathcal{A}_{\mathrm{m}}$. The magnetic

[1]This equality is up to an overall factor of $\psi_0(0)$, which was not accounted for in Sec. 5.1.

amplitude has simple asymptotic behavior; it is linear in x_γ for $x_\gamma \ll \epsilon$ and approximately constant for $x_\gamma \gg \epsilon$

$$\mathcal{A}_{\rm m} \approx \begin{cases} x_\gamma/\epsilon & \text{for } x_\gamma \ll \epsilon \\ 1 & \text{for } x_\gamma \gg \epsilon. \end{cases} \tag{5.22}$$

Therefore, the effective theory spectrum (5.21) is cubic in x_γ in the low-energy limit, $x_\gamma \ll \epsilon$, as required by Low's theorem. Above the hyperfine splitting, $x_\gamma \gg \epsilon$, the spectrum shifts from being cubic in the photon energy to linear.

The ratio of the p-Ps $\to \gamma\nu_\ell\bar{\nu}_\ell$ effective theory to the tree level electroweak spectrum is plotted in Fig. 5.2. In the intermediate energy region ($\epsilon \ll x_\gamma \ll 1$), the ratio plateaus near 1 indicating that the effective theory and tree level electroweak spectrum (2.9) are approximately equal (the two spectra intersect at $x_\gamma \approx 5.75 \times 10^{-5}$). For high-energy photons $x_\gamma \lesssim 1$, the ratio spikes revealing that the effective theory spectrum differs significantly from the tree level electroweak spectrum and is no longer accurate (Fig. 5.2(b)). Below the hyperfine energy splitting, the ratio in the log-log plot is linear with a slope of 2 since the effective theory spectrum is cubic in x_γ while the tree level electroweak spectrum is linear (Fig. 5.2(a)).

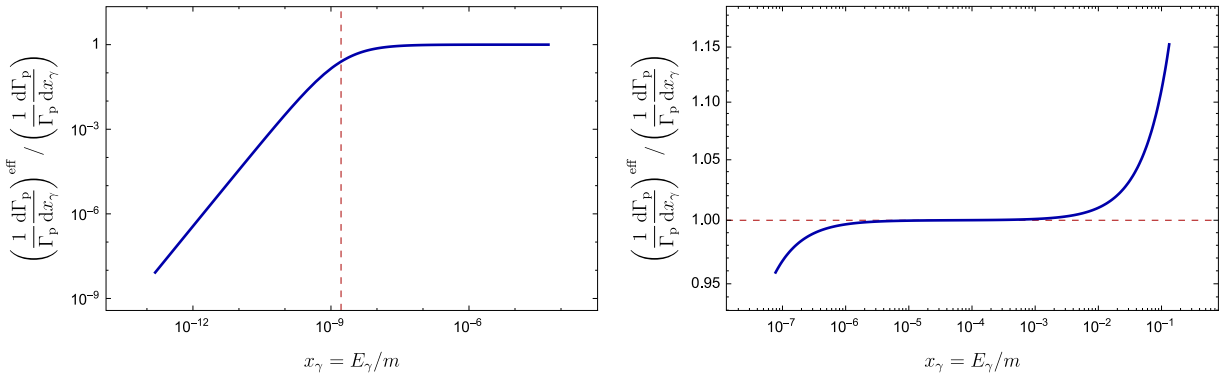

Figure 5.2: Log-log plot of the ratio of the effective theory spectrum to the tree level electroweak spectrum in p-Ps $\to \gamma\nu\bar{\nu}$ decays in (a) the low-energy limit $\alpha^6 < x_\gamma < \alpha^2$ and (b) the high-energy limit $\alpha^3/5 < x_\gamma < 1$. The vertical line in (a) indicates the hyperfine splitting energy ($x_\gamma = \epsilon = 7\alpha^4/12$) while the horizontal line in (b) is placed at 1 to indicate the region where the effective and full theory spectra are equal.

5.4 Soft photon spectrum for o-Ps

In o-Ps $\to \gamma\nu_\ell\bar{\nu}_\ell$ decays, the E1 transition takes the initial o-Ps ground state, 1^3S_1, to the excited o-Ps states $n^3P_{0,1,2}$ ($n \neq 1$), which then decay into a $\nu_\ell\bar{\nu}_\ell$ pair. On the other hand, the M1 transition takes the initial o-Ps state, 1^3S_1, to the p-Ps ground state, 1^1S_0, which cannot decay into a $\nu_\ell\bar{\nu}_\ell$ pair and therefore does not need to be considered.

Thus, the effective theory o-Ps $\to \gamma\nu_\ell\bar{\nu}_\ell$ decay amplitude, Fig. 5.1(b), is given by

$$\begin{aligned}
\mathcal{M}_{\rm o}^{\rm eff} &= \sum_n \frac{i\langle 0|\hat{A}_{\rm p}^{(\nu_\ell\bar{\nu}_\ell)}|n\rangle\langle n|ie\mathbf{x}\cdot\mathbf{E}|\text{o-Ps}\rangle}{E_o - E_n - E_\gamma} \\
&= -2\sqrt{2}i\mathrm{G_F}ea_\ell E_\gamma \sum_n \frac{\langle 0|\,(\mathbf{J}\times\boldsymbol{\sigma})\cdot\mathbf{p}|n\rangle\langle n|\mathbf{x}\cdot\boldsymbol{\epsilon}_\gamma|\text{o-Ps}\rangle}{E_{\rm o} - E_n - E_\gamma},
\end{aligned} \tag{5.23}$$

where $\hat{A}_{\rm p}^{(\nu_\ell\bar{\nu}_\ell)}$ is the p-wave o-Ps $\to \nu_\ell\bar{\nu}_\ell$ annihilation operator (derived in Appendix G),

$$\hat{A}_{\rm p}^{(\nu_\ell\bar{\nu}_\ell)} = -2\sqrt{2}\mathrm{G_F}a_\ell\,(\mathbf{J}\times\boldsymbol{\sigma})\cdot\mathbf{p}. \tag{5.24}$$

As in the calculation of the effective theory p-Ps $\to \gamma\nu_\ell\bar{\nu}_\ell$ amplitude (Sec. 5.3), we now demonstrate that the effective theory amplitude (without binding) is equal to the soft photon limit of the electroweak amplitude. To calculate the effective theory amplitude, ignoring binding effects, we take $E_\gamma \gg m\alpha^2$ and therefore can ignore $E_{\rm o} - E_n$ in the energy denominator of (5.23), which yields

$$\begin{aligned}
\mathcal{M}_{\rm o}^{\rm eff} &\to 2\sqrt{2}i\mathrm{G_F}a_\ell e\sum_n \langle 0|\,(\mathbf{J}\times\boldsymbol{\sigma})\cdot\mathbf{p}|n\rangle\langle n|\mathbf{x}\cdot\boldsymbol{\epsilon}_\gamma|\text{o-Ps}\rangle \\
&= 2\sqrt{2}i\mathrm{G_F}a_\ell e\langle 0|\,(\mathbf{J}\times\boldsymbol{\sigma})\cdot\mathbf{p}\;\mathbf{x}\cdot\boldsymbol{\epsilon}_\gamma|\text{o-Ps}\rangle.
\end{aligned} \tag{5.25}$$

The tensor operator $\mathbf{p}^i\mathbf{x}^j$ can be decomposed into irreducible spherical tensor operators

$$\mathbf{p}^i\mathbf{x}^j = \frac{\delta^{ij}}{3}\mathbf{p}\cdot\mathbf{x} + \frac{\mathbf{p}^i\mathbf{x}^j - \mathbf{p}^j\mathbf{x}^i}{2} + \frac{1}{2}\left(\mathbf{p}^i\mathbf{x}^j + \mathbf{p}^j\mathbf{x}^i - \frac{2}{3}\delta^{ij}\mathbf{p}\cdot\mathbf{x}\right). \tag{5.26}$$

Since the initial o-Ps state is an s-wave, only the operator with zero angular momentum (first term of (5.26)) gives a non-zero matrix element. Additionally, we take the operator $\mathbf{p}$ to act only on $\mathbf{x}$ because $\mathbf{x}\cdot\boldsymbol{\nabla}\psi_0$ vanishes at the origin. With these considerations, the effective theory amplitude (ignoring binding effects) (5.25) simplifies to

$$\mathcal{M}_{\rm o}^{\rm eff} \to 4{\rm G_F} e a_\ell \left(\boldsymbol{\epsilon}_\gamma \times \mathbf{J}\right)\cdot\boldsymbol{\xi}\ \psi_0(0). \tag{5.27}$$

Since this is equal to the soft photon limit of the tree level electroweak amplitude (5.9)[2], the annihilation operator (5.24) and E1 transition fully account for $\nu_\ell\bar{\nu}_\ell$ annihilation and soft photon emission in o-Ps $\to \gamma\nu_\ell\bar{\nu}_\ell$ decays. Thus, equation (5.23) is the complete effective theory amplitude.

We now return to the general case, without any assumptions about photon energies. Expanding the inner products of the effective theory amplitude (5.23), we find

$$\begin{aligned}
\mathcal{M}_{\rm o}^{\rm eff} &= 4{\rm G_F} e a_\ell E_\gamma \left(\mathbf{J}\times\boldsymbol{\xi}\right)^i \boldsymbol{\epsilon}_\gamma^j \int {\rm d}^3x\ {\rm d}^3y\ \delta^{(3)}(\mathbf{x})\ \partial_x^i \left(\sum_n \frac{\langle \boldsymbol{x}|n\rangle\langle n|\boldsymbol{y}\rangle}{E_n+\kappa^2/m}\right) y^j\psi_0(y) \\
&= 4{\rm G_F} e a_\ell E_\gamma \left(\mathbf{J}\times\boldsymbol{\xi}\right)^i \boldsymbol{\epsilon}_\gamma^j \int {\rm d}^3y\ \left[\partial_x^i G_C(\mathbf{x},\mathbf{y},\kappa)\right]_{\mathbf{x}=\mathbf{0}} y^j\psi_0(y)
\end{aligned} \tag{5.28}$$

where $-\kappa^2/m = E_{\rm o} - E_\gamma$ and $G_C(\mathbf{x},\mathbf{y},\kappa)$ is the Coulomb Green's function. The derivative selects the $l=1$ partial wave of the Green's function [24]

$$\left[\partial_x^i G_C(\mathbf{x},\mathbf{y},\kappa)\right]_{\mathbf{x}=\mathbf{0}} = 3y^i G_1(0,y,\kappa). \tag{5.29}$$

where the partial wave decomposition of the Coulomb Green's function can be found in Appendix D of Ref. [22]. Substituting (5.29) into (5.28) and performing the angular

[2]This equality is up to an overall factor of $\psi_0(0)$, which was not accounted for in Sec. 5.1.

integrations yields the effective theory amplitude

$$\begin{aligned}\mathcal{M}_{\rm o}^{\rm eff} &= 4{\rm G_F}ea_\ell\,\psi_0(0)\,(\mathbf{J}\times\boldsymbol{\xi})\cdot\boldsymbol{\epsilon}_\gamma\,\mathcal{A}_e(E_\gamma)\\ &= 4{\rm G_F}ea_\ell\,\psi_0(0)\,(\boldsymbol{\epsilon}_\gamma\times\mathbf{J})\cdot\boldsymbol{\xi}\,\mathcal{A}_e(E_\gamma).\end{aligned}\tag{5.30}$$

Here, the electric amplitude, $\mathcal{A}_{\rm e}$, is

$$\begin{aligned}\mathcal{A}_{\rm e}\left(E_\gamma\right) &= \frac{4\pi E_\gamma}{\psi_0(0)}\int_0^\infty {\rm d}y\, y^4 G_{C,1}\left(0,y;\kappa\right)\psi_0(y)\\ &= \frac{(1-\nu)\,(3+5\nu)}{3\,(1+\nu)^2}+\frac{8\nu^2\,(1-\nu)}{3\,(2-\nu)\,(1+\nu)^3}\,{}_2F_1\left(1,2-\nu;3-\nu;\frac{\nu-1}{\nu+1}\right),\end{aligned}\tag{5.31}$$

where $\nu=\frac{\alpha}{\sqrt{4x_\gamma+\alpha^2}}$. The first line of (5.31), is the same integral representation of the electric amplitude from Ref. [22] while the second line was derived in Ref. [23]. The hypergeometric function ${}_2F_1$ in the second line, simplifies to the so-called Hurwitz-Lerch Φ function [38],

$$\begin{aligned}\frac{1}{2-\nu}\,{}_2F_1\left(1,2-\nu;3-\nu;\frac{\nu-1}{\nu+1}\right) &= \frac{1}{2-\nu}\Phi\left(\frac{\nu-1}{\nu+1},1,2-\nu\right)\\ &= \sum_{n=0}^{\infty}\frac{1}{2-\nu+n}\left(\frac{\nu-1}{\nu+1}\right)^n,\end{aligned}\tag{5.32}$$

$$\mathcal{A}_{\rm e}\left(E_\gamma\right)=\frac{1-\nu}{3\,(1+\nu)^2}\left[3+5\nu+\frac{8\nu^2}{1+\nu}\sum_{n=0}^{\infty}\frac{1}{2-\nu+n}\left(\frac{\nu-1}{\nu+1}\right)^n\right].\tag{5.33}$$

At high energies, equivalent to $x_\gamma\gg\alpha^2$ and $\nu\simeq\frac{\alpha}{2\sqrt{x_\gamma}}\to 0$, this amplitude can be expanded as a series in $\alpha/\sqrt{x_\gamma}$,

$$\mathcal{A}_{\rm e}=1-\frac{2\alpha}{3\sqrt{x_\gamma}}+\frac{(2-2\ln 2)\,\alpha^2}{3x_\gamma}+\ldots,\quad(x_\gamma\gg\alpha^2).\tag{5.34}$$

We see that for $x_\gamma\gg\alpha^2$, the electric amplitude is approximately 1. In this region the binding effects are relatively unimportant. Indeed, the expression (5.30) agrees with the

amplitude obtained when binding effects are ignored, eq. (5.27), when we take $\mathcal{A}_e \to 1$.

On the other hand, in the extreme soft photon limit $x_\gamma \ll \alpha^2$, equivalent to $\nu \simeq 1 - \frac{2x_\gamma}{\alpha^2} \to 1^-$, the electric amplitude can be expanded as a series in x_γ/α^2,

$$\mathcal{A}_{\rm e} = \frac{2x_\gamma}{\alpha^2} + \ldots \quad (x_\gamma \ll \alpha^2). \tag{5.35}$$

The leading term in the soft photon limit is linear in x_γ with a slope of $2/\alpha^2$.

To summarize, the electric amplitude is linear in the photon energy below the binding energy and approximately constant above it. The expansions (5.35) and (5.34) will be important when determining the behaviour of the photon spectrum in the limits $x_\gamma \ll \alpha^2$ and $x_\gamma \gg \alpha^2$.

5.4.1 Low-energy limit and the Stark effect

It is instructive to look for a simple physical connection to the leading low-energy term (5.35). In the soft photon limit, the wavelength is large and the electric field of the wave is approximately constant. This is similar to the situation in the Stark effect. Since the first order correction to the ground state energy for the Stark effect vanishes ($E^{(1)} \propto \langle\psi_0|\mathbf{x}\cdot\boldsymbol{\epsilon}_\gamma|\psi_0\rangle = 0$), one evaluates the second order correction to the ground state energy

$$E^{(2)} = \sum_{n\neq 0} \frac{\langle\psi_0|H'|n\rangle\langle n|H'|\psi_0\rangle}{E_0 - E_n}, \tag{5.36}$$

where $H' \propto \mathbf{x}\cdot\boldsymbol{\epsilon}_\gamma = r\cos\theta$. The form of (5.36) is similar to the low-energy limit of the effective theory amplitude where $E_\gamma = 0$ in the energy denominator of (5.23)

$$\mathcal{M}_{\rm o}^{\rm eff} \;=\; -2\sqrt{2}i{\rm G_F}ea_\ell E_\gamma \sum_n \frac{\langle 0|\,(\mathbf{J}\times\boldsymbol{\sigma})\cdot\mathbf{p}|n\rangle\langle n|\mathbf{x}\cdot\boldsymbol{\epsilon}_\gamma|\text{o-Ps}\rangle}{E_{\rm o} - E_n}. \tag{5.37}$$

Since equation (5.36) can be summed exactly using the method of Dalgarno and Lewis [39, 40], we can exploit the similarity between equations (5.36) and (5.37) to evaluate the

effective theory amplitude in the soft photon limit.

Equations (5.36) and (5.37) can be summed exactly by finding a function F that satisfies

$$[F, H_0]\psi_0(\mathbf{x}) = \mathbf{x}\cdot\boldsymbol{\epsilon}_\gamma\psi_0(\mathbf{x}). \tag{5.38}$$

For the unperturbed positronium Hamiltonian, H_0, the function F is given by

$$F = -\frac{m}{2}\mathbf{x}\cdot\boldsymbol{\epsilon}_\gamma\left(a^2 + \frac{ar}{2}\right) \tag{5.39}$$

where a is the Ps Bohr radius. With F in hand, we evaluate equation (5.37)

$$\begin{aligned}
\mathcal{M}_{\rm o}^{\rm eff} &= -2\sqrt{2}i\mathrm{G_F}ea_\ell E_\gamma\langle 0|\left(\mathbf{J}\times\boldsymbol{\sigma}\right)\cdot\mathbf{p}F|\text{o-Ps}\rangle \\
&= -4\mathrm{G_F}ea_\ell E_\gamma\left(\mathbf{J}\times\boldsymbol{\xi}\right)\cdot\int \mathrm{d}^3x\;\delta^{(3)}(\mathbf{x})\boldsymbol{\nabla}(F\psi_0(\mathbf{x})) \\
&= 4\mathrm{G_F}ea_\ell\;\psi_0(0)\left(\boldsymbol{\epsilon}_\gamma\times\mathbf{J}\right)\cdot\boldsymbol{\xi}\;\frac{2x_\gamma}{\alpha^2}.
\end{aligned} \tag{5.40}$$

Thus, in the limit $x_\gamma \ll \alpha^2$ the electric amplitude is $\mathcal{A}_e \approx 2x_\gamma/\alpha^2$ which is equal to the first order term of the expansion (5.35).

Similarly, the Stark effect can be related to the soft photon limit of the E1 portion of the o-Ps $\to 3\gamma$ decay amplitude. The annihilation operator that contributes to the E1 portion of the o-Ps $\to 3\gamma$ decay amplitude is of the same form as the o-Ps p-wave $\nu_\ell\bar{\nu}_\ell$ annihilation operator and contains a $\mathbf{p}$ derivitive. A calculation, using the summation technique above, reveals that in the soft photon limit, $\mathcal{A}_e \approx 2x_\gamma/\alpha^2$. This agrees with the soft photon limit of the electric amplitude derived in [22, 24] by expansion of the p-wave Green's function.

5.4.2 Photon spectrum

With this understanding of the electric amplitude, we proceed to the the computation of photon spectrum. Both the spin averaged square of the amplitude (5.30) and the three

body phase space in the $x \to 0$ limit are needed. Squaring (5.30), summing over the photon polarizations and averaging over the initial o-Ps polarizations, yields

$$\begin{aligned}\frac{1}{3}\sum_{\boldsymbol{\xi}\boldsymbol{\epsilon}_\gamma}\left|\mathcal{M}_{\rm o}^{\rm eff}\right|^2 &= \frac{1}{3}\sum_{\boldsymbol{\xi}\boldsymbol{\epsilon}_\gamma}\left|4{\rm G_F}ea_\ell\psi_0(0)\mathcal{A}_{\rm e}(E_\gamma)\left(\boldsymbol{\epsilon}_\gamma\times\mathbf{J}\right)\cdot\boldsymbol{\xi}\right|^2 \\ &\underset{x_\gamma\to 0}{\longrightarrow} 128{\rm G_F^2}a_\ell^2\alpha^4m^5\left|\mathcal{A}_{\rm e}(E_\gamma)\right|^2\left(1-\frac{1}{3}\cos^2\theta\right), \end{aligned} \tag{5.41}$$

where $\sum_{\boldsymbol{\xi}\boldsymbol{\epsilon}_\gamma}\left|\left(\boldsymbol{\epsilon}_\gamma\times\mathbf{J}\right)\cdot\boldsymbol{\xi}\right|^2/3 = 16E_1^2\left[1-\frac{1}{3}(\hat{\mathbf{k}}_\gamma\cdot\hat{\mathbf{k}}_1)^2\right]$ (see equation (F.16) in Appendix F), $\hat{\mathbf{k}}_\gamma\cdot\hat{\mathbf{k}}_1 = \cos\theta$ and $E_1 \to m$. Multiplying by the three body phase space in the limit $x_\gamma \to 0$ and integrating over $\cos\theta$ yields the effective theory spectrum

$$\begin{aligned}\left(\frac{1}{\Gamma_{\rm o}}\frac{{\rm d}\Gamma_{\rm o}}{{\rm d}x_\gamma}\right)^{\rm eff} &= \frac{27\pi^3}{8{\rm G_F^2}m^5\alpha^4a_\ell^2}\int_{-1}^{1}{\rm d}\cos\theta\frac{1}{128\pi^3}\frac{x_\gamma}{2}\frac{1}{3}\sum_{\boldsymbol{\xi}\boldsymbol{\epsilon}_\gamma}\left|\mathcal{M}_{\rm o}^{\rm eff}(E_\gamma)\right|^2 \\ &= 3x_\gamma\left|\mathcal{A}_{\rm e}(E_\gamma)\right|^2. \end{aligned} \tag{5.42}$$

The effective theory spectrum is proportional to the square of the electric amplitude and thus shares the same transitional behaviour at $x_\gamma = \alpha^2$. Substituting the leading term from equations (5.35) and (5.34) into (5.42) we obtain the approximate form of the spectrum in the limits $x_\gamma \ll \alpha^2$ and $x_\gamma \gg \alpha^2$

$$\left(\frac{1}{\Gamma_{\rm o}}\frac{{\rm d}\Gamma_{\rm o}}{{\rm d}x_\gamma}\right)^{\rm eff} \approx \begin{cases} \frac{12}{\alpha^2}x_\gamma^3 & \text{for } x_\gamma \ll \alpha^2 \\ 3x_\gamma & \text{for } x_\gamma \gg \alpha^2. \end{cases} \tag{5.43}$$

Clearly, for photons with $x_\gamma \ll \alpha^2$, the spectrum is cubic in the photon energy as required by Low's theorem. For photons in the energy range $\alpha^2 \ll x_\gamma \ll 1$, both the effective theory and tree level electroweak spectra are approximately linear with a slope of 3.

The ratio of the effective theory spectrum to the tree level electroweak spectrum for o-Ps $\to \gamma\nu_\ell\bar{\nu}_\ell$ decays is plotted in Fig. 5.3. The effective theory spectrum and tree level electroweak spectrum are approximately equal in the intermediate energy range $x_\gamma \sim$

$\mathcal{O}(10^{-2} - 10^{-1})$ (Fig. 5.3(b)). For high energy photons the ratio spikes upward indicating that the effective theory spectrum differs significantly from the tree level electroweak spectrum and is no longer accurate (Fig. 5.3(b)). Below the binding energy, the ratio in the log-log plot is linear with a slope of slope of 2 since the effective theory spectrum is cubic in x_γ while the tree level electroweak spectrum is linear (Fig. 5.3(a)).

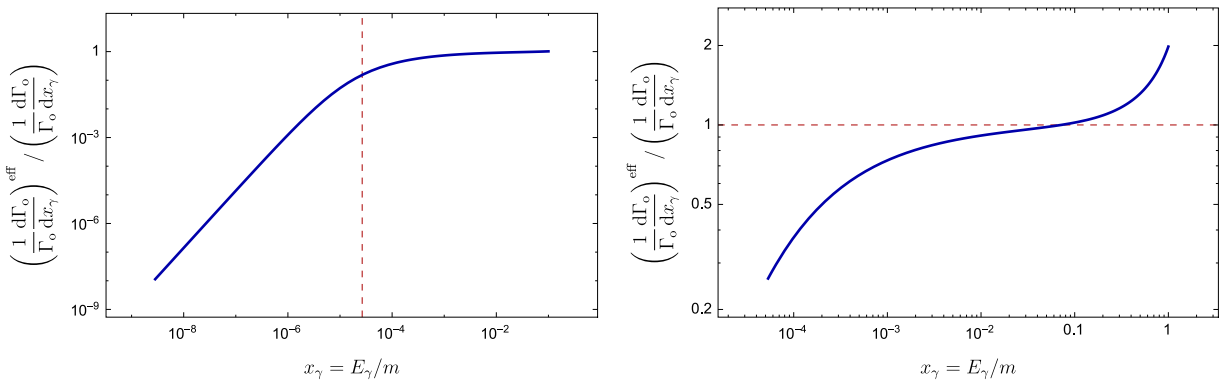

(a) (b)

Figure 5.3: Log-log plot of the ratio of the effective theory spectrum to the tree level electroweak spectrum for o-Ps $\to \gamma\nu\bar{\nu}$ decays in (a) the low-energy limit $\alpha^4 < x_\gamma < 0.1$ and for (b) the high-energy limit $\alpha^2 < x_\gamma < 1$. The vertical line in (a) indicates the binding energy ($x_\gamma = \alpha^2/2$) while the horizontal line in (b) is placed at 1 where the effective theory and electroweak theory spectra are equal.

Chapter 6

Conclusions

We calculated the decay rate and photon spectrum of the decay of Ps into a photon and a neutrino-antineutrino pair (Ps $\to \gamma\nu_\ell\bar{\nu}_\ell$). Both Ps spin states have access to the $\gamma\nu_\ell\bar{\nu}_\ell$ decay channel where the p-Ps and o-Ps final states are orthogonal despite being comprised of the same particles. The decay rates are given by (2.4) and (2.5) and the tree level electroweak photon spectrum by (2.9) and (2.10). These rates and spectra were further examined by calculating the angular dependence of the decay amplitudes, angular distributions and spectra for specific $\gamma + Z^*$ final states (Tables 3.1–3.4).

In principle, this decay could be observed. Experimentally, this channel would appear as the decay of Ps into a single photon if the neutrinos go undetected. However, experimental detection of this channel would be very challenging given the small branching ratios.

The soft photon limit of the tree level electroweak spectra (equations (2.9) and (2.10)) was compared with that predicted by Low's theorem and found to be in disagreement. This contradiction was resolved by including binding effects in the computation of the soft photon spectrum using the methods of non-relativistic effective field theories. The effective theory spectra are given by equations (5.21) and (5.42), and are valid for photon energies much less than the electron mass.

For photon energies much larger than the hyperfine splitting yet still much smaller than the electron rest mass ($m\alpha^4 \ll E_\gamma \ll m$), the p-Ps $\to \gamma\nu_\ell\bar{\nu}_\ell$ effective theory spectrum approaches the tree level electroweak spectrum (2.9). Below the hyperfine splitting ($E_\gamma \ll m\alpha^4$), the effective theory spectrum is cubic in the soft photon energy as required by Low's theorem. In the dipole approximation of the interaction, soft photon p-Ps $\to \gamma\nu_\ell\bar{\nu}_\ell$ decays proceed only by the magnetic M1 transition.

The o-Ps $\to \gamma\nu_\ell\bar{\nu}_\ell$ effective theory spectrum approaches the tree level electroweak spectrum (2.10) for photon energies much larger than the binding energy but still much smaller than the electron rest mass ($m\alpha^2 \ll E_\gamma \ll m$). For photon energies much smaller than the binding energy ($E_\gamma \ll m\alpha^2$), the effective theory spectrum is cubic in the photon energy as required by Low's theorem. In the dipole approximation of the interaction, soft photon o-Ps $\to \gamma\nu_\ell\bar{\nu}_\ell$ decays proceed only by the electric E1 transition.

Lastly, we find connection between the Stark effect and the soft photon limit of the o-Ps $\to \gamma\nu_\ell\bar{\nu}_\ell$ spectrum and the E1 contribution to the o-Ps $\to 3\gamma$ spectrum.

Bibliography

[1] A. Czarnecki, K. Melnikov, and A. Yelkhovsky, Phys. Rev. Lett. **83**, 1135 (1999), hep-ph/9904478.

[2] G. S. Adkins, R. N. Fell, and J. R. Sapirstein, Phys. Rev. Lett. **84**, 5086 (2000), hep-ph/0003028.

[3] A. Czarnecki, K. Melnikov, and A. Yelkhovsky, Phys. Rev. **A61**, 052502 (2000), hep-ph/9910488.

[4] R. J. Hill and G. P. Lepage, Phys. Rev. **D62**, 111301 (2000), hep-ph/0003277.

[5] B. A. Kniehl and A. A. Penin, Phys. Rev. Lett. **85**, 1210 (2000), hep-ph/0004267, [Erratum: Phys. Rev. Lett.85,3065(2000)].

[6] K. Melnikov and A. Yelkhovsky, Phys. Rev. **D62**, 116003 (2000), hep-ph/0008099.

[7] G. S. Adkins, R. N. Fell, and J. Sapirstein, Phys. Rev. **A63**, 032511 (2001).

[8] G. S. Adkins, N. M. McGovern, R. N. Fell, and J. Sapirstein, Phys. Rev. **A68**, 032512 (2003), hep-ph/0305251.

[9] A. A. Penin, Int. J. Mod. Phys. **A19**, 3897 (2004), hep-ph/0308204.

[10] S. G. Karshenboim, Phys. Rept. **422**, 1 (2005), hep-ph/0509010.

[11] B. A. Kniehl, A. V. Kotikov, and O. L. Veretin, Phys. Rev. **A80**, 052501 (2009), 0909.1431.

[12] A. A. Penin, PoS **LL2014**, 074 (2014).

[13] G. S. Adkins, Hyperfine Interact. **233**, 59 (2015).

[14] W. Bernreuther and O. Nachtmann, Z. Phys. **C11**, 235 (1981).

[15] S. Asai, K. Shigekuni, T. Sanuki, and S. Orito, Phys. Lett. **B323**, 90 (1994).

[16] T. Maeno *et al.*, Phys. Lett. **B351**, 574 (1995), hep-ex/9503004.

[17] A. Czarnecki and S. G. Karshenboim, Decays of positronium, in *High Energy Physics and Quantum Field Theory. Proceedings, 14th International Workshop, QFTHEP'99, Moscow, Russia, May 27-June 2, 1999*, pp. 538–544, 1999, hep-ph/9911410.

[18] P. Crivelli, Int. J. Mod. Phys. **A19**, 3819 (2004).

[19] A. Badertscher *et al.*, Phys. Rev. **D75**, 032004 (2007), hep-ex/0609059.

[20] J. Pérez-Ríos and S. T. Love, J. Phys. **B48**, 244009 (2015), 1508.01144.

[21] J. Pestieau and C. Smith, Phys. Lett. **B524**, 395 (2002), hep-ph/0111264.

[22] A. V. Manohar and P. Ruiz-Femenia, Phys. Rev. **D69**, 053003 (2004), hep-ph/0311002.

[23] M. B. Voloshin, Mod. Phys. Lett. **A19**, 181 (2004), hep-ph/0311204.

[24] P. D. Ruiz-Femenia, Nucl. Phys. **B788**, 21 (2008), 0705.1330.

[25] F. E. Low, Phys. Rev. **110**, 974 (1958).

[26] D. J. Griffiths, *Introduction to Quantum Mechanics* (Cambridge University Press, 2016).

[27] M. Srednicki, *Quantum Field Theory* (Cambridge University Press, 2007).

[28] S. Weinberg, *The Quantum Theory of Fields: Volume 1, Foundations* (Cambridge University Press, 2005).

[29] M. E. Peskin and D. V. Schroeder, *An Introduction to Quantum Field Theory* (Addison-Wesley, 1995).

[30] M. D. Harpen, Med. Phys. **31**, 57 (2004).

[31] J. Pirenne, Arch. Sci. Phys. Nat. **29** (1947).

[32] A. Ore and J. L. Powell, Phys. Rev. **75**, 1696 (1949).

[33] W. J. Marciano, Phys. Rev. **D60**, 093006 (1999), hep-ph/9903451.

[34] A. Czarnecki, K. Melnikov, and A. Yelkhovsky, Phys. Rev. **A59**, 4316 (1999), hep-ph/9901394.

[35] A. Czarnecki and W. J. Marciano, Nature **435**, 437 (2005).

[36] R. P. Feynman, R. B. Leighton, and M. Sands, *The Feynman Lectures on Physics* (Addison-Wesley, 1963).

[37] R. Dick, *Advanced Quantum Mechanics: Materials and Photons* (Springer International Publishing, 2016).

[38] F. W. J. Olver, D. W. Lozier, R. F. Boisvert, and C. W. Clark, editors, *NIST Handbook of Mathematical Functions* (Cambridge University Press, 2011).

[39] C. Schwartz, Ann. Phys. **2**, 156 (1959).

[40] A. Dalgarno and J. T. Lewis, Proceedings of the Royal Society of London A: Mathematical, Physical and Engineering Sciences **233**, 70 (1955).

[41] M. Jacob and G. C. Wick, Annals Phys. **7**, 404 (1959).

[42] S. U. Chung, Report No. CERN-71-08 (1971).

[43] J. D. Richman, Report No. CALT-68-1148 (1984).

[44] E. Leader, Camb. Monogr. Part. Phys. Nucl. Phys. Cosmol. **15** (2011).

[45] M. E. Rose, *Elementary Theory of Angular Momentum* (John Wiley & Sons, 1957).

[46] M. D. Schwartz, *Quantum Field Theory and the Standard Model* (Cambridge University Press, 2014).

Appendix A

Factorization of the three-body phase space

A three-body phase space can be factorized into two two-body phase spaces and an integral over an invariant mass squared. Specifically for Ps $\to \gamma\nu_\ell\bar{\nu}_\ell$ decays, the three body Ps $\to \gamma\nu_\ell\bar{\nu}_\ell$ phase space is factorized into two two- body phase spaces (one for Ps $\to \gamma Z^*$ and one for $Z^* \to \nu\bar{\nu}$) and an integral over the invariant mass of Z^* squared. In Sec. A.1, we review two-body phases spaces – the basis for this factorization. Then we derive the three-body factorization for three massive particles and take the limit relevant for our decay where all three particles are massless (Sec. A.2).

A.1 Two-body phase spaces

In general, the N-body phase space measure is given by [29]

$$\mathrm{d}\Phi_N\left(P^\mu; k_1, ..., k_N\right) = (2\pi)^4\,\delta^{(4)}\left(P^\mu - \sum_{i=1}^{N} k_i^\mu\right)\prod_{i=1}^{N}\frac{\mathrm{d}^3 k_i}{(2\pi)^3}\frac{1}{2E_i}. \tag{A.1}$$

Here, P^μ is the total 4-momentum of all initial particles, and, k_i and E_i are the 4-momentum and energy of the i^{th} particle in the final state. Since the integration measure,

$\mathrm{d}^3k_i/(2\pi)^3 2E_i$, is Lorentz invariant, the integrals in each two-body phase space can be performed in any inertial reference frame.

For the two-body phase space, we choose to work in the center of mass frame of the initial particles so that the total 4-momentum is given by $P^\mu = \sum_i p_i^\mu = (\sqrt{s}, \mathbf{0})$ where $s = P \cdot P$ is the invariant mass squared and p_i is the 4-momentum of the i^{th} particle in the initial state. Denoting the masses and 4-momentum of the final state particles by m_1, k_1 and m_2, k_2, the phase space volume is

$$\begin{aligned} \int d\Phi_2(P; k_1, k_2) &= \int \frac{\mathrm{d}^3k_1}{2E_1\,(2\pi)^3} \frac{\mathrm{d}^3k_2}{2E_2\,(2\pi)^3} (2\pi)^4\, \delta^{(4)}\left(P^\mu - k_1^\mu - k_2^\mu\right) \\ &= \frac{\tilde{\beta}(s; m_1^2, m_2^2)}{8\pi} \int \frac{d\cos\theta_1}{2} \frac{d\phi_1}{2\pi}. \end{aligned} \tag{A.2}$$

In the equation above, the function $\tilde{\beta}$ is

$$\tilde{\beta}\left(s; s_1, s_2\right) = \sqrt{1 - \frac{2\left(s_1 + s_2\right)}{s} + \frac{\left(s_1 - s_2\right)^2}{s^2}}. \tag{A.3}$$

In the case where the final state particles are massless, $\tilde{\beta}$ simplifies to unity. For the case $m_1 = m_2 = m$,

$$\tilde{\beta}(s, m^2, m^2) = \sqrt{1 - \frac{4m^2}{s}} = \sqrt{1 - \frac{m^2}{E^2}}, \tag{A.4}$$

which is the velocity of a final state particle.

A.2 Three-body phase space factorization

We first determine the three-body phase space factorization assuming massive final state particles with masses $m_1, m_2,$ and m_3, and 4-momenta $k_1, k_2,$ and k_3. Once we have the three-body factorization for massive particles, we specialize to the massless limit relevant for our decay.

Starting with the three-body phase space,

$$\int \mathrm{d}\Phi_3\left(P;k_1,k_2,k_3\right) = \int \left(\prod_{i=1}^{3} \frac{\mathrm{d}^3 k_i}{\left(2\pi\right)^3 2E_i}\right) \left(2\pi\right)^4 \delta^{(4)}\left(P-k_1-k_2-k_3\right), \tag{A.5}$$

we insert unity in the form of the integral

$$1 = \int \frac{\mathrm{d}^4 q_{12}}{\left(2\pi\right)^4} \left(2\pi\right)^4 \delta^{(4)}\left(q_{12}-p_1-p_2\right) \Theta\left(q_{12}^0\right) \tag{A.6}$$

where $q_{12} = k_1 + k_2$. Even though the step function eliminates half of the integral over q_{12}^0, the delta function ensures that q_{12}^0 is given by the sum of two energies and hence its support (all points of a function which are non-zero) is in the half retained. In addition to inserting unity in the form of (A.6), we also insert

$$1 = \int \frac{\mathrm{d}s_{12}}{2\pi} 2\pi\delta\left(s_{12}-q_{12}^2\right). \tag{A.7}$$

The delta functions in (A.6) and (A.7) allow for the identification of s_{12} as the "mass squared" of the "particle" whose 4-momentum is q_{12}. For the Ps $\to \gamma\nu_\ell\bar{\nu}_\ell$ decay, q_{12} is the 4-momentum of the effective vector boson Z^* and s_{12} is the Z^* invariant mass squared.

Multiplying (A.6) and (A.7) together and performing the energy integral yields

$$\begin{aligned} 1 &= \int \frac{\mathrm{d}^4 q_{12}}{\left(2\pi\right)^4} \frac{\mathrm{d}s_{12}}{2\pi} \left(2\pi\right)^4 \delta^{(4)}\left(q_{12}-p_1-p_2\right) \Theta\left(q_{12}^0\right) 2\pi\delta\left(s_{12}-q_{12}^2\right) \\ &= \int \frac{\mathrm{d}^3 q_{12}}{\left(2\pi\right)^3 2E_{12}} \frac{\mathrm{d}s_{12}}{2\pi} \left(2\pi\right)^4 \delta^{(4)}\left(q_{12}-p_1-p_2\right). \end{aligned} \tag{A.8}$$

In the first line of equation (A.8), the delta function $\delta(s_{12}-q_{12}^2)$ sets $s_{12} = E_{12}^2 - \mathbf{q}_{12}^2$ while the step function $\Theta(q_{12}^0)$ ensures that $q_{12}^0 = +\sqrt{s_{12}+\mathbf{q}_{12}^2}$. Inserting equation (A.8) into the three-body phase space, (A.5), yields the three-body factorization

$$\int \mathrm{d}\Phi_3\left(P;k_1,k_2,k_3\right) = \int \frac{\mathrm{d}s_{12}}{2\pi} \mathrm{d}\Phi_2\left(P;q_{12},k_3\right) \mathrm{d}\Phi_2\left(q_{12};k_1,k_2\right). \tag{A.9}$$

Or in terms of the function, $\tilde{\beta}$,

$$\begin{aligned}\int \mathrm{d}\Phi_3\left(P;k_1,k_2,k_3\right) &= \int \frac{\mathrm{d}s_{12}}{2\pi}\int \frac{\mathrm{d}\cos\theta_3}{2}\frac{\mathrm{d}\phi_3}{2\pi}\frac{\tilde{\beta}\left(s,s_{12},m_3^2\right)}{8\pi} \\ &\quad\times\int \frac{\mathrm{d}\cos\theta_{12}}{2}\frac{\mathrm{d}\phi_{12}}{2\pi}\frac{\tilde{\beta}\left(s_{12};m_1^2,m_2^2\right)}{8\pi}. \end{aligned} \tag{A.10}$$

In the massless limit, $m_1 = m_2 = m_3 = 0$, the three-body phase space factorization simplifies to

$$\begin{aligned}\int \mathrm{d}\Phi_3\left(P;k_1,k_2,k_3\right) &= \int \frac{\mathrm{d}s_{12}}{2\pi}\mathrm{d}\Phi_2\left(P;q_{12},k_3\right)\mathrm{d}\Phi_2\left(q_{12};k_1,k_2\right) \\ &= \left(\frac{1}{8\pi}\right)^2\int \frac{\mathrm{d}s_{12}}{2\pi}\int \frac{\mathrm{d}\cos\theta_3}{2}\frac{\mathrm{d}\phi_3}{2\pi}\left(1-\frac{s_{12}}{s}\right) \\ &\quad\times\int \frac{\mathrm{d}\cos\theta_{12}}{2}\frac{\mathrm{d}\phi_{12}}{2\pi}. \end{aligned} \tag{A.11}$$

This is the factorization referenced in chapter 3. It is used in appendix B to formulate the three-body Ps $\to \gamma\nu_\ell\bar{\nu}_\ell$ decay in terms of a two-body Ps $\to \gamma Z^*$ decay.

Appendix B

Formulation of the Ps $\to \gamma\nu_\ell\bar{\nu}_\ell$ decay rate in terms of γ and Z^*

To rewrite the Ps $\to \gamma\nu_\ell\bar{\nu}_\ell$ decay rate in terms of the Ps $\to \gamma Z^*$ decay rate, we start with the Ps $\to \gamma\nu_\ell\bar{\nu}_\ell$ decay amplitude and then factorize the three-body ($\gamma\nu_\ell\bar{\nu}_\ell$) phase into two two-body phase spaces (γZ^* and $\nu_\ell\bar{\nu}_\ell$) as detailed in Appendix A. Performing the integrals in the $\nu_\ell\bar{\nu}_\ell$ phase space yields the Ps $\to \gamma\nu_\ell\bar{\nu}_\ell$ decay rate in terms of the Ps $\to \gamma Z^*$ decay rate.

The Feynman diagrams relevant for the Ps $\to \gamma\nu_\ell\bar{\nu}_\ell$ decay are illustrated in Fig. 2. As in chapter 2, we neglect the 3-momentum of the incoming leptons as well as the virtual W- and Z-bosons. With these approximations, the p/o-Ps $\to \gamma\nu_\ell\bar{\nu}_\ell$ amplitudes are

$$i\mathcal{M}_{\mathrm{p/o}} = \frac{i\mathrm{G_F}}{\sqrt{2\pi\alpha}}(\epsilon_\gamma)^*_\mu g_{\nu\rho}\mathrm{Tr}\left[X^{\mu\nu}_{\mathrm{p/o}}(p_1,k_\gamma)\right]J^\rho(k_1,k_2), \tag{B.1}$$

where

$$\begin{aligned} X^{\mu\nu}_{\mathrm{p/o}}(p_1,k_\gamma) = \mathrm{Tr}\Bigg[2m\Psi_{\mathrm{p/o}}\Bigg((ie)\gamma^\nu\left(v_\ell - a_\ell\gamma^5\right)\frac{\not{p}_1 - \not{k}_\gamma + m}{(p_1-k_\gamma)^2-m^2}(-ie)\gamma^\mu \\ +(-ie)\gamma^\mu\frac{\not{k}_\gamma - \not{p}_2 + m}{(k_\gamma-p_2)^2-m^2}(ie)\gamma^\nu\left(v_\ell - a_\ell\gamma^5\right)\Bigg)\Bigg], \end{aligned} \tag{B.2}$$

and $J^{\mu}\left(k_1,k_2\right)=\bar{u}(k_1)\gamma^{\mu}\left(1-\gamma^5\right)v(k_2)$ is the neutral weak current. The p-Ps and o-Ps projection operators are given by $\Psi_{\rm p}=\left(1+\gamma^0\right)\gamma^5/(2\sqrt{2})$ and $\Psi_{\rm o}=\left(1+\gamma^0\right)\boldsymbol{\gamma}\cdot\boldsymbol{\xi}/(2\sqrt{2})$ where $\boldsymbol{\xi}$ is the o-Ps polarization vector [34].

To calculate the Ps $\to\gamma\nu_\ell\bar{\nu}_\ell$ decay rate, we start from the standard formula,

$$\Gamma_{\rm p/o} \;=\; \frac{1}{2m_{\rm Ps}}\int {\rm d}\Phi_3(p_1+p_2;k_1,k_2,k_\gamma)\frac{\left|\psi_0(0)\right|^2}{m}\frac{1}{g}\sum_{\rm spin/pol}\left|\mathcal{M}_{\rm p/o}\right|^2, \qquad \text{(B.3)}$$

where $\psi_0(0)$ is the ground state positronium wave function at the origin and g is the number of Ps polarizations of the initial state [29].

Substituting the three-body spin averaged matrix element squared

$$\sum_{\rm spin/pol}\left|\mathcal{M}_{\rm p/o}\right|^2 \;=\; g_{\alpha\beta}g_{\mu\rho}g_{\nu\sigma}\frac{{\rm G_F^2}}{2\pi\alpha}X_{\rm p/o}^{\alpha\mu}X_{\rm p/o}^{\beta\nu\,*}{\rm Tr}\left[\not{k}_1\gamma^\rho(1-\gamma^5)\not{k}_2\gamma^\sigma(1-\gamma^5)\right], \quad \text{(B.4)}$$

into (B.3) and factorizing the three-body phase space into two two-body phase spaces (Appendix A), yields the decay rate

$$\begin{aligned}\Gamma_{\rm p/o} \;=\; & \frac{1}{2m_{\rm Ps}}\int\frac{{\rm d}s}{2\pi}{\rm d}\Phi_2(2p_1;k_\gamma,q)\frac{\left|\psi_{\rm Ps}(0)\right|^2}{m}\frac{g_{\alpha\beta}g_{\mu\rho}g_{\nu\sigma}}{g}\frac{{\rm G_F^2}}{2\pi\alpha}X_{\rm p/o}^{\alpha\mu}X_{\rm p/o}^{\beta\nu\,*}\\ & \int{\rm d}\Phi_2(q;k_1,k_2)k_{1\eta}k_{2\lambda}{\rm Tr}\left[\gamma^\eta\gamma^\rho(1-\gamma^5)\gamma^\lambda\gamma^\sigma(1-\gamma^5)\right], \qquad \text{(B.5)}\end{aligned}$$

where $s=q\cdot q$ is the invariant mass of Z^* squared and q is its 4-momentum. The neutrino phase space integral can be performed by writing the neutrino momentum product, $k_{1\eta}k_{2\lambda}$, as a linear combination of the only available tensors, $k_{1\eta}k_{2\lambda}=Aq^2g_{\eta\lambda}+Bq_\eta q_\lambda$. The momentum conserving delta function in ${\rm d}\Phi_2(q;k_1,k_2)$ forces $q=k_1+k_2$. A system of equations for A and B is obtained by contracting $\int{\rm d}\Phi_2(q;k_1,k_2)k_{1\eta}k_{2\lambda}$ with $g^{\eta\lambda}$ and $q^\eta q^\lambda$, and yields the solution $A=1/12$ and $B=1/6$. Thus, the neutrino contribution to

the decay rate is

$$\int \mathrm{d}\Phi_2(q;k_1,k_2)k_{1\eta}k_{2\lambda}\mathrm{Tr}\left[\gamma^\eta\gamma^\rho(1-\gamma^5)\gamma^\lambda\gamma^\sigma(1-\gamma^5)\right] = \frac{1}{3\pi}\left[q^\rho q^\sigma - q^2 g^{\rho\sigma}\right]$$
$$= \frac{1}{3\pi}q^2\sum_s \epsilon_s^\rho(q)\epsilon_s^{\sigma *}(q), \qquad \text{(B.6)}$$

where the sum over the polarizations of a massive vector boson is given by

$$\sum_s \epsilon_s^\rho(q)\epsilon_s^{\sigma *}(q) = \frac{q^\rho q^\sigma}{q^2} - g^{\rho\sigma}. \qquad \text{(B.7)}$$

Substituting (B.6) into equation (B.5), we obtain the Ps $\to \gamma\nu_\ell\bar{\nu}_\ell$ decay rate in terms of Ps $\to \gamma Z^*$

$$\begin{aligned}
\Gamma_{\mathrm{p/o}} &= \frac{1}{2m_{\mathrm{Ps}}}\int \frac{\mathrm{d}s}{2\pi}\mathrm{d}\Phi_2(2p_1;k_\gamma,q)\frac{|\psi_{Ps}(0)|^2}{m}\frac{g_{\alpha\beta}}{g}\frac{\mathrm{G_F^2}}{2\pi\alpha}X_{\mathrm{p/o}}^{\alpha\mu}X_{\mathrm{p/o}}^{\beta\nu\,*}\frac{1}{3\pi}q^2\sum_s(\epsilon_s)_\mu(\epsilon_s^*)_\nu \\
&= \frac{\mathrm{G_F^2}}{2\pi^2\alpha}\int\frac{\mathrm{d}q^2}{2\pi}q^2\left(\frac{1}{2m_{\mathrm{Ps}}}\int\mathrm{d}\Phi_2(2p;k_\gamma,q)\frac{|\psi_{Ps}(0)|^2}{m}\frac{1}{3g}\sum_{\mathrm{pol}}\left|\mathcal{M}_{\mathrm{p/o\text{-}Ps}\to\gamma Z^*}\right|^2\right) \\
&= \frac{\mathrm{G_F^2}}{2\pi^2\alpha}\int\frac{\mathrm{d}q^2}{2\pi}q^2\Gamma_{\mathrm{p/o\text{-}Ps}\to\gamma Z^*}. \qquad \text{(B.8)}
\end{aligned}$$

Appendix C

Calculation of Ps $\to \gamma Z^*$ decay amplitudes along the z-axis

Given that the Ps $\to \gamma\nu_\ell\bar{\nu}_\ell$ decay can be written in terms of Ps $\to \gamma Z^*$ (equation (3.1)), we now determine the Ps $\to \gamma Z^*$ amplitudes for decay along the z-axis. These amplitudes are used in chapter 3 to construct the full angular dependence of the Ps $\to \gamma Z^*$ amplitudes.

The relevant diagrams for Ps $\to \gamma Z^*$ decays are given in Fig C.1. As in chapter 2, we approximate the electron and positron to be at rest with initial 4-momentum $p = p_1 = p_2 = (m, \mathbf{0})$. The 4-momentum of the photon is k_γ while the 4-momentum of the Z^* is q.

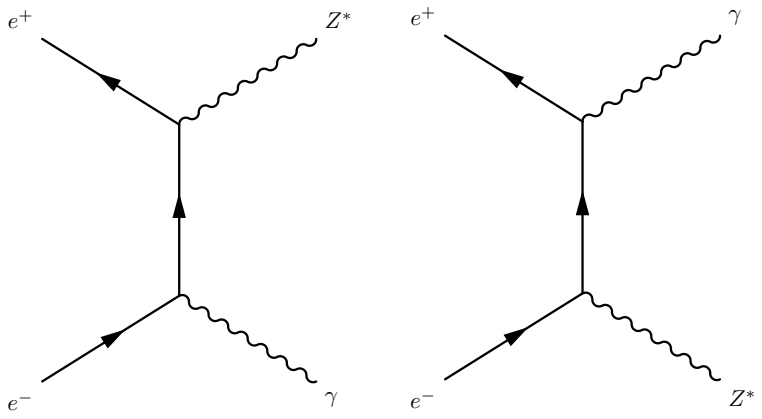

Figure C.1: The relevant Feynman diagrams for the two-body decay, Ps $\to \gamma Z^*$.

As discussed in chapter 3, the Z^* couples to the electron with Feynman rule $ie\not{\epsilon}(q)^*(v_\ell - a_\ell\gamma^5)$. The matrix elements for Ps $\to \gamma Z^*$ are

$$\begin{aligned} i\mathcal{M}_{\text{p/o-Ps}\to\gamma Z^*} = \bar{v}(p) \Bigg[& ie\not{\epsilon}^*(q)(v_\ell - a_\ell\gamma^5)\frac{i\left(\not{p} - \not{k}_\gamma + m\right)}{(p-k_\gamma)^2 - m^2}(-ie)\not{\epsilon}^*(k_\gamma) \\ & + (-ie)\not{\epsilon}^*(k_\gamma)\frac{i\left(\not{p} - \not{q} + m\right)}{(p-q)^2 - m^2}ie\not{\epsilon}^*(q)\left(v_\ell - a_\ell\gamma^5\right)\Bigg] u(p) \\ = 2mie^2\text{Tr}\Bigg[\Psi_{\text{p/o}}\Bigg(& \not{\epsilon}^*(q)(v_\ell - a_\ell\gamma^5)\frac{(\not{p} - \not{k}_\gamma + m)}{(p-k_\gamma)^2 - m^2}\not{\epsilon}^*(k_\gamma) \\ & + \not{\epsilon}^*(k_\gamma)\frac{(\not{p} - \not{q} + m)}{(p-q)^2 - m^2}\not{\epsilon}^*(q)\left(v_\ell - a_\ell\gamma^5\right)\Bigg)\Bigg]. \end{aligned} \tag{C.1}$$

We can simplify (C.1) by performing the trace. This yields the two-body amplitudes

$$i\mathcal{M}_{\text{p/o-Ps}\to\gamma Z^*} = \begin{cases} \frac{-4i}{\sqrt{2}}\frac{v_\ell e^2}{mE_\gamma}\varepsilon_{\alpha\beta\gamma\delta}p^\alpha k_\gamma^\beta \epsilon^{*\gamma}(k_\gamma)\epsilon^{*\delta}(q) & \text{for p-Ps} \\ \frac{-4i}{\sqrt{2}}\frac{a_\ell e^2}{E_\gamma}\varepsilon_{\alpha\beta\gamma\delta}k^\alpha \epsilon^{*\beta}(k_\gamma)\epsilon^{*\gamma}(q)\xi^\delta & \text{for o-Ps} \end{cases} \tag{C.2}$$

where $\xi = (0, \boldsymbol{\xi})$ is the polarization of the o-Ps state and ε is the totally anti-symmetric Levi-Civita tensor.

To simplify equation (C.2), we need to understand the properties of polarizations for both massless and massive spin-one particles (Appendix C.1). In sections C.2 and C.3, we simplify (C.2) for p-Ps and o-Ps decays.

C.1 Spin-one polarizations

Consider a spin-one particle moving along the z-axis with 4-momentum $p = (E, \mathbf{p})$. The transverse polarizations,

$$\epsilon_\pm = \mp\frac{1}{\sqrt{2}}(0, 1, \pm i, 0), \tag{C.3}$$

$$\epsilon_\pm^* = \mp\frac{1}{\sqrt{2}}(0, 1, \mp i, 0), \tag{C.4}$$

are available to both massive and massless bosons. The longitudinal polarization,

$$\epsilon_0 = \frac{1}{\sqrt{s}}(|\mathbf{p}|, 0, 0, E) = \epsilon_0^*, \tag{C.5}$$

is, however, only accessible to massive bosons. In the above equation, $\sqrt{s} = \sqrt{p \cdot p}$ is the invariant mass of the boson.

The contractions with the Levi-Civita tensor in (C.2) can be simplified to a sum of ordinary 3-dimensional vector products. The necessary vector products for the simplification of equation (C.2) are listed below:

$$\epsilon_\pm^* \times \epsilon_\pm^* = 0, \tag{C.6}$$

$$\boldsymbol{\epsilon}_\pm^* \times \boldsymbol{\epsilon}_\mp^* = \left(\mp\frac{1}{\sqrt{2}}(1, \mp i, 0)\right) \times \left(\pm\frac{1}{\sqrt{2}}(1, \pm i, 0)\right) = \mp i\hat{\mathbf{z}}, \tag{C.7}$$

$$\hat{\mathbf{z}} \times \boldsymbol{\epsilon}_\pm^* = (0, 0, 1) \times \mp\frac{1}{\sqrt{2}}(1, \mp i, 0) = \pm i\boldsymbol{\epsilon}_\pm^*. \tag{C.8}$$

C.2 Amplitudes for p-Ps along the z-axis

Simplifying the contractions with the Levi-Civita tensor in equation (C.2), the p-Ps$\to$ γZ^* amplitude is

$$i\mathcal{M}_{\text{p-Ps}\to\gamma Z^*} = -\frac{4i}{\sqrt{2}}\frac{v_\ell e^2}{E_\gamma}\mathbf{k}_\gamma \cdot [\boldsymbol{\epsilon}^*(k_\gamma) \times \boldsymbol{\epsilon}^*(q)] \tag{C.9}$$

where the photon is moving in the $+z$-direction with 4-momentum $k_\gamma = (E_\gamma, E_\gamma\hat{\mathbf{z}})$ and the Z^* is moving in the $-z$-direction with 4-momentum $q = (E_Z, -E_\gamma\hat{\mathbf{z}})$.

The amplitudes, where Z^* has a transverse polarization, are

$$i\mathcal{M}_{\text{p-Ps}\to\gamma Z^*} = \begin{cases} \mp\frac{4v_\ell e^2}{\sqrt{2}} & \text{for } \boldsymbol{\epsilon}(k_\gamma) = \boldsymbol{\epsilon}^\pm \text{ and } \boldsymbol{\epsilon}(q) = \boldsymbol{\epsilon}^\mp, \\ 0 & \text{for } \boldsymbol{\epsilon}(k_\gamma) = \boldsymbol{\epsilon}^\pm \text{ and } \boldsymbol{\epsilon}(q) = \boldsymbol{\epsilon}^\pm. \end{cases} \tag{C.10}$$

The amplitudes, where Z^* has a longitudinal polarization ($\boldsymbol{\epsilon}(k_\gamma) = \boldsymbol{\epsilon}^\pm$ and $\boldsymbol{\epsilon}(q) = \boldsymbol{\epsilon}_0$), are

$$i\mathcal{M}_{\text{p-Ps}\to\gamma Z^*} = \frac{\mp 4 v_\ell e^2}{\sqrt{2}} \frac{E_Z}{\sqrt{s} E_\gamma} \left(\mathbf{k}_\gamma \cdot \boldsymbol{\epsilon}^*_\pm\right) = 0. \tag{C.11}$$

Since the amplitude in (C.11) vanishes, p-Ps can only decay into a Z^* with a transverse polarization.

For convenience, we define the non-zero amplitudes to be

$$B_{\pm\mp} \equiv \mathcal{M}_{\text{p-Ps}\to\gamma Z^*}|_{\boldsymbol{\epsilon}(k_\gamma)=\boldsymbol{\epsilon}^\pm \text{ and } \boldsymbol{\epsilon}(q)=\boldsymbol{\epsilon}^\mp} = \pm i \frac{4 v_\ell e^2}{\sqrt{2}}. \tag{C.12}$$

C.3 Amplitudes for o-Ps along the z-axis

Simplifying the contractions with the Levi-Civita tensor in equation (C.2), the o-Ps$\to$ γZ^* amplitude is

$$i\mathcal{M}_{\text{o-Ps}\to\gamma Z^*} = -\frac{4 i a_\ell e^2}{\sqrt{2}} \left\{ E_\gamma \boldsymbol{\xi} \cdot [\boldsymbol{\epsilon}^*(k_\gamma) \times \boldsymbol{\epsilon}^*(q)] + \epsilon^{*0}(q) \boldsymbol{\xi} \cdot [\hat{\mathbf{z}} \times \boldsymbol{\epsilon}^*(k_\gamma)] \right\}. \tag{C.13}$$

where the photon is moving in the $+z$-direction with 4-momentum $k_\gamma = (E_\gamma, E_\gamma \hat{\mathbf{z}})$ and the Z^* is moving in the $-z$-direction with 4-momentum $q = (E_Z, -E_\gamma \hat{\mathbf{z}})$.

The amplitudes, where Z^* has a transverse polarization, are

$$\begin{aligned} i\mathcal{M}_{\text{o-Ps}\to\gamma Z^*} &= -\frac{4 i a_\ell e^2}{\sqrt{2}} \boldsymbol{\xi} \cdot [\boldsymbol{\epsilon}(k_\gamma) \times \boldsymbol{\epsilon}(q)] \\ &= \begin{cases} \pm \frac{4 i a_\ell e^2}{\sqrt{2}} \boldsymbol{\xi} \cdot \hat{\mathbf{z}} & \text{for } \boldsymbol{\epsilon}(k_\gamma) = \boldsymbol{\epsilon}^\pm \text{ and } \boldsymbol{\epsilon}(q) = \boldsymbol{\epsilon}^\mp, \\ 0 & \text{for } \boldsymbol{\epsilon}(k_\gamma) = \boldsymbol{\epsilon}^\pm \text{ and } \boldsymbol{\epsilon}(q) = \boldsymbol{\epsilon}^\pm. \end{cases} \end{aligned} \tag{C.14}$$

The amplitudes, where Z^* has a longitudinal polarization ($\boldsymbol{\epsilon}(k_\gamma) = \boldsymbol{\epsilon}^\pm$ and $\boldsymbol{\epsilon}(q) = \boldsymbol{\epsilon}_0$),

are

$$\begin{aligned} i\mathcal{M}_{\text{o-Ps}\to\gamma Z^*} &= -\frac{4ia_\ell e^2}{\sqrt{2}}\left\{\boldsymbol{\xi}\cdot\left[\boldsymbol{\epsilon}_\pm^*\times\boldsymbol{\epsilon}^*(q)\right]+\epsilon^{*0}\boldsymbol{\xi}\cdot\left[\hat{\mathbf{z}}\times\boldsymbol{\epsilon}_\pm^*\right]\right\} \\ &= -\frac{4ia_\ell e^2}{\sqrt{2}}\left[\boldsymbol{\xi}\cdot\left(\boldsymbol{\epsilon}_\pm^*\times\frac{-E_Z\hat{\mathbf{z}}}{\sqrt{s}}\right)+\frac{E_\gamma}{\sqrt{s}}\boldsymbol{\xi}\cdot\left(\hat{\mathbf{z}}\times\boldsymbol{\epsilon}_\pm^*\right)\right] \\ &= \frac{\pm 4a_\ell e^2}{\sqrt{2}}\frac{E_\gamma+E_Z}{\sqrt{s}}\boldsymbol{\xi}\cdot\boldsymbol{\epsilon}_\pm^*. \end{aligned} \tag{C.15}$$

Unlike p-Ps, o-Ps can decay into a Z^* with either a transverse or longitudinal polarization.

For convenience, we define the non-zero amplitudes to be

$$A_{\pm\mp} \equiv \mathcal{M}_{\text{o-Ps}\to\gamma Z^*}\big|_{\boldsymbol{\epsilon}(k_\gamma)=\boldsymbol{\epsilon}^\pm \text{ and } \boldsymbol{\epsilon}(q)=\boldsymbol{\epsilon}^\mp} = \pm\frac{4ia_\ell e^2}{\sqrt{2}}\boldsymbol{\xi}\cdot\hat{\mathbf{z}}, \tag{C.16}$$

$$A_{\pm 0} \equiv \mathcal{M}_{\text{o-Ps}\to\gamma Z^*}\big|_{\boldsymbol{\epsilon}(k_\gamma)=\boldsymbol{\epsilon}^\pm \text{ and } \boldsymbol{\epsilon}(q)=\boldsymbol{\epsilon}^0} = \frac{\pm 4a_\ell e^2}{\sqrt{2}}\frac{E_\gamma+E_Z}{\sqrt{s}}\boldsymbol{\xi}\cdot\boldsymbol{\epsilon}_\pm^*. \tag{C.17}$$

Appendix D

Derivation of the o-Ps amplitudes with their angular dependence

Initially, the o-Ps atom is in a state of definite angular momentum denoted by $|\Lambda\rangle$. Since o-Ps and its decay products, γ and Z^*, are all spin one particles, we abbreviate the angular momentum states $|1, m_s\rangle$ by $|m_s\rangle$ where m_s is the projection of spin along the z-axis. The massive Z^* boson has access to all three spin projection states (i.e., $m_Z \in \{\pm 1, 0\}$) while the massless photon cannot access the longitudinally polarized $|0\rangle$ state (i.e., $m_\gamma \in \{\pm 1\}$). Conservation of angular momentum requires that the spin projection quantum numbers satisfy $m_\gamma + m_Z = m_\Lambda$; as a result, there are four different modes in which o-Ps can decay along the z-axis.

Consider $|\Lambda\rangle$ initially polarized in the state $|+\rangle$ along the z-axis. Since the photon must have $m_\gamma = \pm 1$, conservation of angular momentum implies $|\gamma\rangle = |+\rangle$ and $|Z^*\rangle = |0\rangle$; we assign the amplitude A_{+0} to this decay. If $|\Lambda\rangle$ is initially polarized in the state $|-\rangle$, $|\gamma\rangle = |-\rangle$ and $|Z^*\rangle = |0\rangle$; we assign the amplitude A_{-0} to this decay. Lastly, if $|\Lambda\rangle$ is initially polarized in the state $|0\rangle$, $m_\gamma = -m_Z$ and therefore $|\gamma\rangle = |\pm\rangle$ and $|Z^*\rangle = |\mp\rangle$; we assign amplitudes $A_{\pm\mp}$ to these decays.

From Appendix C, the o-Ps $\to \gamma Z^*$ amplitudes along the z-axis are

$$A_{\pm 0} = \pm\frac{4e^2 a_\ell}{\sqrt{2}}\frac{E_\gamma + E_Z}{q}\boldsymbol{\xi}\cdot\boldsymbol{\epsilon}_\pm^* = \pm\frac{4e^2 a_\ell}{\sqrt{2}}\frac{E_\gamma + E_Z}{q}\delta_{m_\Lambda,\pm}, \tag{D.1}$$

$$A_{\pm\mp} = \pm\frac{4ie^2 a_\ell}{\sqrt{2}}\boldsymbol{\xi}\cdot\hat{\mathbf{z}} = \pm\frac{4ie^2 a_\ell}{\sqrt{2}}\delta_{m_\Lambda,0}, \tag{D.2}$$

where $\boldsymbol{\epsilon}_\pm$ are the transverse polarization vectors of the photon and $\boldsymbol{\xi}$ is the o-Ps polarization vector. Here q is the momentum of the Z^*.

To determine the angular dependence of the decay amplitudes on the spherical angles, θ and ϕ, we consider two coordinate systems $\{x, y, z\}$ and $\{x', y', z'\}$. The z'-axis is defined by the angles θ and ϕ in the $\{x, y, z\}$ coordinate system and represents the decay axis. The angular dependence of the decay amplitudes is constructed by rotating the initial o-Ps state and then considering the decay into $\gamma + Z^*$ along z'.

The combination of rotations required to bring $\{x, y, z\}$ onto $\{x', y', z'\}$ (Fig. D.1) is

$$R = R_{z'}(\alpha)R_{y'}(\theta)R_{z'}(\phi), \tag{D.3}$$

where $R_{\mathbf{n}}(\theta) = e^{i\theta\mathbf{n}\cdot\mathbf{S}}$ is the operator for rotations about the axis given by the unit vector, $\mathbf{n}$, and $\mathbf{S} = (S_x, S_y, S_z)$ is the spin-one matrix operator [37].

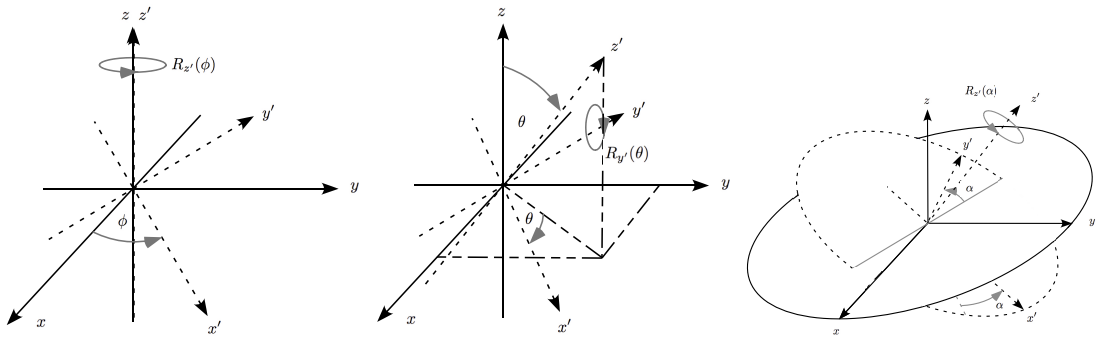

Figure D.1: Sequence of rotations transforming $\{x, y, z\}$ (solid) to $\{x', y', z'\}$ (dashed).

Application of R to $|\Lambda\rangle$ yields the amplitude for $|\Lambda\rangle$ to be in the state $|m'_\Lambda\rangle$ along the z'-axis for each $m'_\Lambda \in \{\pm 1, 0\}$. If $|\Lambda\rangle$ is initially polarized in the state $|+\rangle$, then $|\Lambda\rangle$ has an

amplitude of $\frac{1}{2}(1+\cos\theta)e^{i\alpha}e^{i\phi}$ to be in the state $|+'\rangle$ (the $m_\Lambda = 1$ state along the z' axis). If $|\Lambda\rangle$ is in the state $|+'\rangle$, it decays to $|+'; k\hat{\mathbf{z}}'\rangle_\gamma \otimes |0'; -k\hat{\mathbf{z}}'\rangle_Z$ with an amplitude $A_{+'0'}$, where k is the magnitude of the photon momentum along z'. Thus, the total amplitude for the decay of an o-Ps atom with spin projection $m_\Lambda = +1$ into a photon moving along $+z'$-axis with spin projection $m'_\gamma = +1$ is

$$\mathcal{A}^{+}_{+'0'}(\theta,\phi) = \frac{A_{+'0'}}{2}(1+\cos\theta)e^{i\alpha}e^{i\phi}. \tag{D.4}$$

Similarly, the amplitude for the final state $|-'; k\hat{\mathbf{z}}'\rangle_\gamma \otimes |0'; -k\hat{\mathbf{z}}'\rangle_Z$ is

$$\mathcal{A}^{+}_{-'0'}(\theta,\phi) = \frac{A_{-'0'}}{2}(1-\cos\theta)e^{-i\alpha}e^{i\phi}, \tag{D.5}$$

and the amplitudes for $|\pm'; k\hat{\mathbf{z}}'\rangle_\gamma \otimes |\mp'; -k\hat{\mathbf{z}}'\rangle_Z$ are

$$\mathcal{A}^{+}_{\pm'\mp'}(\theta,\phi) = \frac{-A_{\pm'\mp'}}{\sqrt{2}}\sin\theta e^{i\phi}. \tag{D.6}$$

We denote the o-Ps decay amplitudes with their full angular dependencies as $\mathcal{A}^{m_\Lambda}_{m'_\gamma m'_Z}$ where $m_\Lambda \in \{\pm1, 0\}$ is the initial spin projection of o-Ps along the z-axis, and, $m'_\gamma \in \{\pm1\}$ and $m'_Z \in \{\pm1, 0\}$ are the spin projections of the photon and Z^* along the z'-axis. The amplitudes, $\mathcal{A}^{0}_{m'_\gamma m'_Z}$, are obtained using the method outlined above while $\mathcal{A}^{-}_{m'_\gamma m'_Z}$ is obtained from $\mathcal{A}^{+}_{m'_\gamma m'_Z}$ by the prescription $\theta \to \theta+\pi$, $\phi \to -\phi$ and $\alpha \to -\alpha$. The o-Ps amplitudes, $\mathcal{A}^{m_\Lambda}_{m'_\gamma m'_Z}$, are listed in table 3.2 where we have chosen the convention $\alpha = 0$.

Appendix E

Angular dependence of the o-Ps amplitudes: helicity basis formalism

The angular dependence of the o-Ps amplitudes (chapter 3) can be determined using the helicity basis formalism of [41, 42, 43, 44] instead of the method outlined in Appendix D. The helicity basis formalism, provides a simple and powerful method to analyze two-body reactions involving particles of arbitrary spin; it also applies equally well to relativistic particles. This formalism uses states of definite helicity (states where angular momentum and spin are quantized along the direction of linear momentum) as a basis instead of states of definite angular momentum. States of definite helicity are particularly useful because they are invariant under rotations; the quantization axis rotates with the system.

The initial o-Ps state is one of definite total angular momentum

$$|i\rangle \equiv |\mathbf{p}_i = 0; 1m_\lambda\rangle \tag{E.1}$$

where $\mathbf{p}_i$ is the initial momentum of the o-Ps atom and m_Λ is the o-Ps spin projection along the z-axis. In terms of the relativistic plane-wave state, $|P_i\rangle$, the initial o-Ps state is

$$|i\rangle = |1m_\Lambda\rangle|P_i = 0\rangle \tag{E.2}$$

where P_i is the initial 4-momentum of the o-Ps state.

We express the final, γZ^*, state as a two-particle plane-wave state of definite helicity in the center of mass frame. These particles move back-to-back with momentum of magnitude $|\mathbf{p}_f|$ along the decay axis (the axis along which the decay products move). The helicities of the two final state particles are the spin projections along the decay axis. The total helicity is $\lambda = \lambda_\gamma - \lambda_Z$ where λ_γ and λ_Z are the helicities of the photon and Z^*. This final state can be expressed as

$$|f\rangle \propto |\theta_f \phi_f \lambda_\gamma \lambda_Z\rangle |P_f\rangle \tag{E.3}$$

where $|\theta_f \phi_f \lambda_\gamma \lambda_Z\rangle$ is a two particle plane wave helicity state, θ_f is the polar angle of the decay axis and ϕ_f is the azimuthal angle of the decay axis.

The o-Ps $\to \gamma Z^*$ decay amplitude, up to an overall multiplicative constant and the energy-momentum conserving δ-function is given by

$$\mathcal{A}_{m_\Lambda \lambda}(i \to f) \propto \langle \theta_f \phi_f \lambda_\gamma \lambda_Z | \hat{U} | 1 m_\Lambda \rangle \tag{E.4}$$

where the operator $\hat{U}$ governs the annihilation of positronium into γZ^*.

In order to take advantage of conservation of angular momentum in the amplitude (E.4), we need to know how to write states of definite angular momentum, J, and spin projection, M, in terms of helicity states. Namely,

$$|JM\lambda_1\lambda_2\rangle = \sqrt{\frac{2J+1}{4\pi}} \int_0^{2\pi} d\phi \int_{-1}^{1} d\cos\theta D^{J*}_{M\lambda=\lambda_1-\lambda_2}(\phi, \theta, 0) |\theta\phi\lambda_1\lambda_2\rangle \tag{E.5}$$

where $D^j_{m'm}$ is the Wigner D function (see chapter 13 of Ref. [45] for a definition of the Wigner D functions and their properties). After inserting unity in the form of

$$1 = \sum_{JM} |JM\lambda_\gamma\lambda_Z\rangle\langle JM\lambda_\gamma\lambda_Z| \tag{E.6}$$

into (E.4) the amplitude becomes

$$\begin{aligned}\mathcal{A}_{m_\Lambda\lambda}(i\to f) &= \sum_{JM}\langle\theta_f\phi_f\lambda_\gamma\lambda_Z|JM\lambda_\gamma\lambda_Z\rangle\langle JM\lambda_\gamma\lambda_Z|\hat{U}|1m_\Lambda\rangle \\ &= \sum_{JM}\sqrt{\frac{2J+1}{4\pi}}D^{J*}_{M\lambda}(\phi_f,\theta_f,0)\delta_{J,1}\delta_{M,m_\Lambda}\langle\lambda_1\lambda_2|U|1m_\Lambda\rangle \\ &= \sqrt{\frac{3}{4\pi}}D^{1*}_{m_\Lambda\lambda}(\phi_f,\theta_f,0)A_{\lambda_\gamma\lambda_Z} \qquad \text{(E.7)}\end{aligned}$$

where $A_{\lambda_\gamma\lambda_Z} = \langle 1\lambda_\gamma\lambda_Z|\hat{U}|1m_s\rangle$ is called the helicity amplitude. Since all the angular dependance comes from the Wigner D functions, equation (E.7) may be used to verify the angular dependence of the o-Ps amplitudes in chapter 3 (Table 3.2) without determining the helicity amplitude, $A_{\lambda_\gamma\lambda_Z}$ (Table E.1).

Table E.1: Table of the Wigner D functions, $D^{1*}_{m_\Lambda\lambda}(\phi,\theta,0)$, needed to evaluate the decay Ps $\to \gamma\nu_\ell\bar{\nu}_\ell$ decay amplitudes in the helicity basis formalism. Here, m_Λ is the spin projection of o-Ps along the z-axis and $\lambda = m'_\gamma + m'_Z$ is the total helicity where, like in chapter 3, m'_γ and m'_Z are the spin projections of the photon and Z^* along the decay axis (z'-axis). The Wigner D functions for $m_\Lambda = -1$ are obtained by the replacement $\theta \to \theta + \pi$ and $\phi \to -\phi$. Furthermore, only configurations of m_Λ, m'_γ and m'_Z that conserve angular momentum are defined.

		m'_Z		
m_Λ	m'_γ	$+1$	0	-1
$+1$	$+1$	0	$(1+\cos\theta)e^{i\phi}/2$	$-\sin\theta e^{i\phi}/\sqrt{2}$
	-1	$-\sin\theta e^{i\phi}/\sqrt{2}$	$(1-\cos\theta)e^{i\phi}/2$	0
0	$+1$	0	$\sin\theta/\sqrt{2}$	$\cos\theta$
	-1	$\cos\theta$	$-\sin\theta/\sqrt{2}$	0

Appendix F

The neutral weak current

In order to evaluate the extreme soft photon limit of the Ps $\to \gamma\nu_\ell\bar{\nu}_\ell$ amplitudes (chapter 5) and the Ps $\to \nu_\ell\bar{\nu}_\ell$ annihilation operators (Appendix G), we calculate the explicit expression for the neutral weak current,

$$J^\mu = \bar{u}(k_1)\gamma^\mu(1-\gamma^5)v(k_2) = 2\bar{u}(k_1)\gamma^\mu P_L v(k_2) \tag{F.1}$$

where k_1 (k_2) is the neutrino (antineutrino) 4-momentum and $P_L = (1-\gamma^5)/2$ is the left handed projection operator. Additionally, we utilize some properties of J^μ to simplify the polarization sums in the spin averaged Ps $\to \gamma\nu_\ell\bar{\nu}_\ell$ amplitudes squared, equations (5.20) and (5.41).

In order to provide the most apparent connection to non-relativistic quantum mechanics, we use Dirac spinors for the electron and positron as well as the Dirac representation of the gamma matrices (chapter 5). However, expressing the neutral weak current using Dirac spinors for neutrinos is cumbersome because Dirac spinors are eigenstates of the spin operator not the left handed projection operator, P_L. Therefore, we choose to use spinors of definite handedness (chirality), the so-called Weyl spinors, to determine J^μ.

Left handed Weyl spinors transform in the irreducible $(\frac{1}{2}, 0)$ representation of the Lorentz group while right handed Weyl spinors transform in the irreducible $(0, \frac{1}{2})$ repre-

sentation [46]. Left/right handed Weyl spinors are eigenstates of the left/right handed projection operators[1], $P_L = (1-\gamma^5)/2$ and $P_R = (1+\gamma^5)/2$.

Additionally, the representation of the gamma matrices in the neutral weak current is irrelevant because J^μ is a 4-vector and has no spinor indices. Therefore, we also use the Weyl representation of the gamma matrices because the Weyl spinors are especially simple (only two non-zero components) [29].

In the Weyl representation, the left and right handed spinors for massless neutrinos of 4-momentum $k = (E, k_x, k_y, k_z)$ are

$$u_L(k) = \frac{1}{\sqrt{E+k_z}} \begin{pmatrix} -k_x + ik_y \\ k_z + E \\ 0 \\ 0 \end{pmatrix}, \tag{F.2}$$

$$u_R(k) = \frac{1}{\sqrt{E+k_z}} \begin{pmatrix} 0 \\ 0 \\ k_z + E \\ k_x + ik_y \end{pmatrix} \tag{F.3}$$

where $E = |\mathbf{k}|$ (derived by solving problem 3.3 of [29]). As always, the anti-particle spinors are obtained from the charge conjugation operation

$$v_L(k) = -i\gamma^2 u_L^*(k) \tag{F.4}$$

$$v_R(k) = -i\gamma^2 u_R^*(k). \tag{F.5}$$

For the calculations of chapter 5, we only need the current in the limit that the photon energy in $\mathrm{Ps} \to \gamma\nu_\ell\bar{\nu}_\ell$ decays vanishes, $E_\gamma \to 0$ (i.e., when the neutrinos move

[1]Since neutrinos are (nearly) massless, the Weyl spinors for neutrinos are also eigenstates of the helicity operator (spin projection along the direction of motion).

back-to-back: $\mathbf{k}_2 = -\mathbf{k}_1$ and $E_2 = E_1$). Therefore,

$$\begin{aligned} J^\mu(k_1,k_2)|_{\mathbf{k}_2=-\mathbf{k}_1 \text{ and } E_2=E_1} &= 2\bar{u}(k_1)\gamma^\mu P_L v(k_2)|_{\mathbf{k}_2=-\mathbf{k}_1 \text{ and } E_2=E_1} \\ &= 2\bar{u}_L(k_1)\gamma^\mu v_R(k_2)|_{\mathbf{k}_2=-\mathbf{k}_1 \text{ and } E_2=E_1} \\ &= \frac{4}{\sqrt{E_1^2-k_{1z}^2}} \begin{pmatrix} 0 \\ -k_{1x}k_{1z} - ik_{1y}E_1 \\ -k_{1y}k_{1z} + ik_{1x}E_1 \\ E_1^2 - k_{1z}^2 \end{pmatrix}. \end{aligned} \tag{F.6}$$

Since $J^0 = 0$ in the $E_\gamma \to 0$ limit, many of the computations in chapter 5 are simplified. Furthermore, 3-vector dot products involving the spatial part of the current satisfy the simple identities

$$\mathbf{J}\cdot\mathbf{J}^* = 32\left|\mathbf{k}_1\right|^2, \tag{F.7}$$

$$(\mathbf{r}\cdot\mathbf{J})(\mathbf{r}\cdot\mathbf{J}^*) = 16\left|\mathbf{r}\right|^2\left|\mathbf{k}_1\right|^2 - 16\left(\mathbf{k}_1\cdot\mathbf{r}\right)^2, \tag{F.8}$$

for any $\mathbf{r}\in\mathbb{R}^3$.

We will use equations (F.7) and (F.8) to simplify equations (5.20) and (5.41). Specifically, we want to simplify

$$\sum_{\boldsymbol{\epsilon}_\gamma} |\left(\boldsymbol{\epsilon}_\gamma \times \mathbf{J}\right)\cdot\hat{\mathbf{k}}_\gamma|^2, \tag{F.9}$$

for the p-Ps spectrum and

$$\frac{1}{3}\sum_{\boldsymbol{\xi}\boldsymbol{\epsilon}_\gamma} |\left(\boldsymbol{\epsilon}_\gamma \times \mathbf{J}\right)\cdot\boldsymbol{\xi}|^2, \tag{F.10}$$

for the o-Ps spectrum. Here, $\boldsymbol{\epsilon}_\gamma$ is the photon polarization 3-vector, $\hat{\mathbf{k}}_\gamma = \mathbf{k}_\gamma/E_\gamma$ is the unit momentum 3-vector of the photon and $\boldsymbol{\xi}$ is the o-Ps polarization 3-vector.

Simplifying the polarization sums in (F.9) and (F.10) yields

$$\sum_{\boldsymbol{\epsilon}_\gamma} |\left(\boldsymbol{\epsilon}_\gamma \times \mathbf{J}\right) \cdot \hat{\mathbf{k}}_\gamma|^2 = |\mathbf{J}|^2 - |\mathbf{J} \cdot \hat{\mathbf{k}}_\gamma|^2, \tag{F.11}$$

$$\frac{1}{3}\sum_{\boldsymbol{\xi}\boldsymbol{\epsilon}_\gamma} |\left(\boldsymbol{\epsilon}_\gamma \times \mathbf{J}\right) \cdot \boldsymbol{\xi}|^2 = |\mathbf{J}|^2 - \frac{1}{3}|\mathbf{J} \cdot \hat{\mathbf{k}}_\gamma|^2 \tag{F.12}$$

where we have used the identities [22]

$$\sum_{\boldsymbol{\epsilon}_\gamma} \boldsymbol{\epsilon}_{\gamma i}\boldsymbol{\epsilon}_{\gamma j}^* = \delta_{ij} - \hat{\mathbf{k}}_{\gamma i}\hat{\mathbf{k}}_{\gamma j}, \tag{F.13}$$

$$\sum_{\boldsymbol{\xi}} \boldsymbol{\xi}_i\boldsymbol{\xi}_j^* = \delta_{ij}. \tag{F.14}$$

Using the identities (F.7) and (F.8) in equations (F.11) and (F.12), we get the fully simplified polarization sums required for equations (5.20) and (5.41)

$$\sum_{\boldsymbol{\epsilon}_\gamma} |\left(\boldsymbol{\epsilon}_\gamma \times \mathbf{J}\right) \cdot \hat{\mathbf{k}}_\gamma|^2 = 16E_1^2\left[1 + (\hat{\mathbf{k}}_\gamma \cdot \hat{\mathbf{k}}_1)^2\right], \tag{F.15}$$

$$\frac{1}{3}\sum_{\boldsymbol{\xi}\boldsymbol{\epsilon}_\gamma} |\left(\boldsymbol{\epsilon}_\gamma \times \mathbf{J}\right) \cdot \boldsymbol{\xi}|^2 = 16E_1^2\left[1 - \frac{1}{3}(\hat{\mathbf{k}}_\gamma \cdot \hat{\mathbf{k}}_1)^2\right], \tag{F.16}$$

where $\hat{\mathbf{k}}_1 = \mathbf{k}_1/E_1$ is the unit momentum 3-vector of the neutrino.

Appendix G

Derivation of the o-Ps $\to \nu\bar{\nu}$ annihilation operator

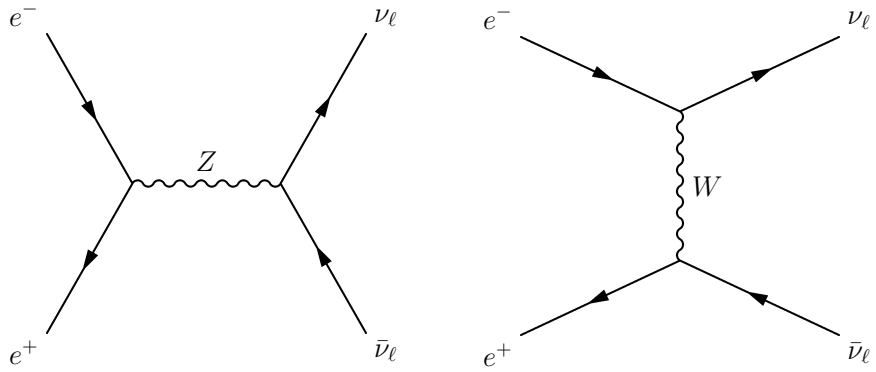

Figure G.1: The $e^+e^- \to \nu_\ell\bar{\nu}_\ell$ annihilation graphs for (a) Z boson exchange and (b) W boson exchange. The graph (a) contributes to the Ps $\to \nu_\ell\bar{\nu}_\ell$ amplitude for all lepton flavours $\ell = e, \mu, \tau$ while (b) only contributes when $\ell = e$.

In order to calculate the effective theory amplitudes (chapter 5), we require the $\mathcal{O}(|\mathbf{p}|/m)$ expansion of the $e^+e^- \to \nu_\ell\bar{\nu}_\ell$ annihilation amplitude (Fig. G.1). The electron and positron 4-momentum are $p_1 = (E, \mathbf{p})$ and $p_2 = (E, -\mathbf{p})$ while the neutrino and

anti-neutrino 4-momentum are k_1 and k_2. The amplitude of Fig. G.1 is

$$\begin{aligned} A^{(\nu_\ell\bar{\nu}_\ell)} &= -i\sqrt{2}\mathrm{G_F}\bar{v}(-\mathbf{p})\not{J}(v_\ell - a_\ell\gamma^5)u(\mathbf{p}) \\ &= 2\sqrt{2}i\mathrm{G_F}m\ \chi^\dagger\left[\begin{pmatrix} \frac{(\boldsymbol{\sigma}\cdot\mathbf{p})^\dagger}{2mc} & 1 \end{pmatrix}\not{J}\left(v_\ell - a_\ell\gamma^5\right)\begin{pmatrix} 1 \\ \frac{\boldsymbol{\sigma}\cdot\mathbf{p}}{2mc} \end{pmatrix}\right]\phi \\ &= \chi^\dagger\hat{A}^{(\nu_\ell\bar{\nu}_\ell)}\phi, \end{aligned} \tag{G.1}$$

where

$$\hat{A}^{(\nu_\ell\bar{\nu}_\ell)} = 2\sqrt{2}i\mathrm{G_F}m\begin{pmatrix} \frac{\boldsymbol{\sigma}\cdot\mathbf{p}}{2m} & 1 \end{pmatrix}\begin{pmatrix} J_0 & -\mathbf{J}\cdot\boldsymbol{\sigma} \\ \mathbf{J}\cdot\boldsymbol{\sigma} & -J_0 \end{pmatrix}\begin{pmatrix} v_\ell & -a_\ell \\ -a_\ell & v_\ell \end{pmatrix}\begin{pmatrix} 1 \\ \frac{\boldsymbol{\sigma}\cdot\mathbf{p}}{2m} \end{pmatrix} \tag{G.2}$$

is the $\nu_\ell\bar{\nu}_\ell$ annihilation operator. From momentum conservation, $\mathbf{k}_1 = -\mathbf{k}_2$, the time component of the neutral weak current vanishes, $J_0 = 0$. Therefore, the $\nu_\ell\bar{\nu}_\ell$ annihilation operator becomes

$$\hat{A}^{(\nu_\ell\bar{\nu}_\ell)} = 2\sqrt{2}i\mathrm{G_F}mv_\ell\left(\mathbf{J}\cdot\boldsymbol{\sigma}\right) - 2\sqrt{2}\mathrm{G_F}a_\ell\left(\mathbf{J}\times\boldsymbol{\sigma}\right)\cdot\mathbf{p}. \tag{G.3}$$

The first term of equation (G.3), proportional to vector coupling, is the s-wave o-Ps $\to$ $\nu_\ell\bar{\nu}_\ell$ annihilation operator

$$\hat{A}_{\mathrm{s}}^{(\nu_\ell\bar{\nu}_\ell)} = 2\sqrt{2}i\mathrm{G_F}mv_\ell\left(\mathbf{J}\cdot\boldsymbol{\sigma}\right). \tag{G.4}$$

In the computation of the p-Ps $\to \gamma\nu_\ell\bar{\nu}_\ell$ effective theory amplitude, the s-wave annihilation operator takes the intermediate s-wave o-Ps state into a neutrino-antineutrino pair. The second term, proportional to axial coupling, is the p-wave o-Ps $\to \nu_\ell\bar{\nu}_\ell$ annihilation operator

$$\hat{A}_{\mathrm{p}}^{(\nu_\ell\bar{\nu}_\ell)} = -2\sqrt{2}\mathrm{G_F}a_\ell\left(\mathbf{J}\times\boldsymbol{\sigma}\right)\cdot\mathbf{p}. \tag{G.5}$$

In the computation of the o-Ps $\to \gamma\nu_\ell\bar{\nu}_\ell$ effective theory amplitude, the p-wave annihilation operator takes the intermediate p-wave o-Ps states into a neutrino-antineutrino pair.